All Aligned on the Western Front of North America? Analyzing the Stress Field in the Northern Cordillera

T. Stephan[1,2] and **E. Enkelmann**[2]

[1]Department of Geology, Lakehead University, Thunder Bay, ON, Canada, [2]Department of Geoscience, University of Calgary, Calgary, AB, Canada

Abstract This study presents the first rigorous statistical analysis of the present-day crustal stress along the western margin of the North American Plate, covering the entire Canadian Cordillera and Alaska. Using circular statistics and geometric tests, we develop a regional stress province model that constrains the directions of first-order stresses. Observed stresses from the World Stress Map database and other published sources are compared with modeled directions derived from plate boundary stresses, mantle drag, and gravitation-induced body forces. Our results show that plate boundary forces dominate the stress field, particularly those associated with the convergent and transform boundaries between the Pacific/Yakutat and North American plates. Local stress modifications are caused by slip partitioning related to oblique plate boundary geometries. Active regions at the northeastern edge of the Cordillera coincide with the superposition of stresses from both the Pacific–North American transform boundary and the Arctic/North Atlantic ridge push. Despite their large distance from active plate boundaries, the alignment of stress trajectories in the Richardson Mountains and Mackenzie Mountains results in stress amplification and eventually deformation. Conversely, misalignment and hence stress reduction explains the seismic quiescence in the Canadian Rocky Mountains. Thereby, the lithospheric-scale structural inheritance along the Tintina Fault and the northern Rocky Mountain Trench acts a major deflector of far-field stresses. Second-order drivers, notably gravitation-induced body forces, further modify stress fields, particularly along the northern slope of the Brooks Range and within the North American foreland of the Cascadia subduction zone.

Plain Language Summary The Earth's crust is shaped by geological forces, known as stresses, which control how the ground moves, shakes or rises to form mountains. We analyze the stresses that act along the western edge of the North American Plate, covering the Canadian Cordillera and Alaska. By combining data from many sources and using new statistical methods, we develop a large-scale model to understand how stress is distributed across such a vast region. Our findings show that most stresses derive from forces generated at the boundaries of plates by their movements, particularly where the Pacific plate collides with North America. The geometry of these boundaries and gravity create local changes of the stresses. Even areas far from these boundaries, such as the Richardson and Mackenzie Mountains, are still strongly affected when boundary stresses from the Pacific and the distant Arctic edge of North America combine. By contrast, where stresses cancel each other out, such as in parts of the Canadian Rockies, the crust is relatively quiet. We also discovered that some deep faults in the Cordillera's crust redirect stress over long distances. Together, these findings help to explain why some regions experience frequent earthquakes and mountain building while others do not.

1. Introduction

What drives deformation in the Cordilleran orogen? The Aleutian-Alaska-Canadian Cordillera is the result of subduction, terrane accretion, and transform motion that started more than 200 Myr ago and is still active today (Figure 1). Currently, this diffuse plate boundary zone is characterized by widespread active deformation and high topography reaching >800 km inboard of the active Pacific plate boundary over a generally thin and hot lithosphere (Hyndman & Currie, 2011). Seismicity occurs primarily along the active plate boundaries at the western margin of North America and extends far into the continental interior in Alaska, northern Canada and contiguous US, but not in southern Canada (Figure 1). A striking feature is the existence of large areas lacking notable seismicity (i.e., magnitudes below 4), such as between the eastern Denali and the Tintina faults in the Yukon (Figure 1). The seismic pattern indicates shortening on both sides of these seismic gaps, raising questions on how plate boundary stresses are transmitted through the lithosphere and how they interplay with other major forces.
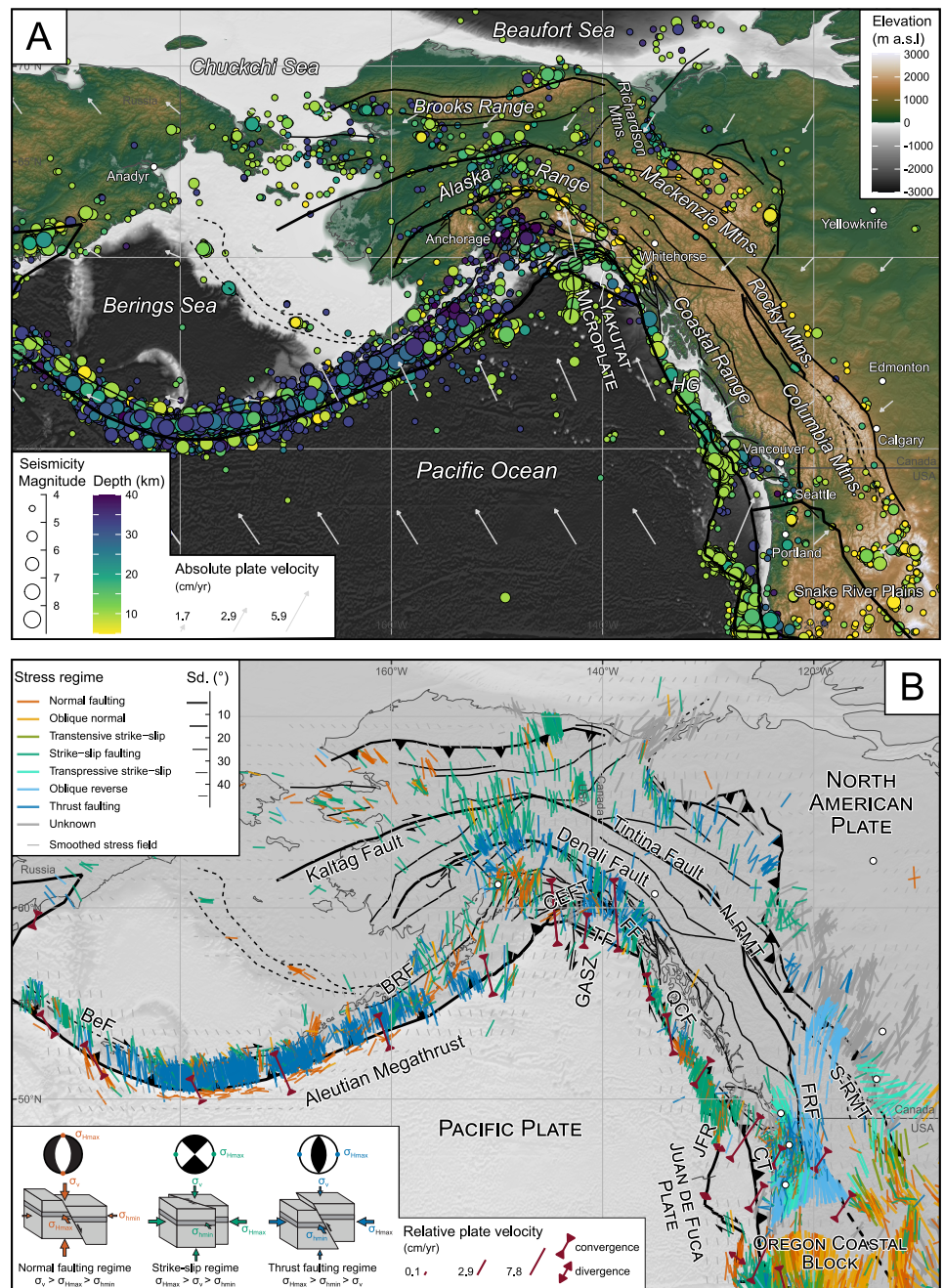
Figure 1. Tectonic map of Alaska and the Canadian Cordillera. (a) Crustal seismicity since 1970 showing epicenters for earthquakes between 5 and 40 km depth and magnitude $M_w > 4$ (compiled from ANSS catalog, Guy et al., 2016). Gray arrows depict the vectors of absolute motion (HS3-NUVEL, Gripp & Gordon, 2002). Elevation data are based on the ETOPO1 model (NOAA National Geophysical Data Center, 2009). HG—Haida Gwaii. (b) Structures and observed stress field. Colored bars give orientation of the maximum horizontal stress σ_{Hmax} and the stress regime compiled from the World Stress Map Database Release 2025 and other sources (see text for details). Gray bars show the smoothed stress field. Bold black and gray lines are major faults and cratonic shear zones, respectively. BeF—Bering Fault, BRF—Border Ranges Fault, CT—Cascadia Megathrust, CEFT—Chugach-St. Elias Fold-and-Thrust Belt, FF—Fairweather Fault, FRF—Fraser River Fault, GASZ—Gulf of Alaska Shear Zone, QCF—Queen Charlotte Fault, RMT—Rocky Mountain Trench (N—Northern, S—Southern), TF—Transition Fault.

Understanding the kinematics within this diffuse plate boundary zone requires knowledge of the relative contribution of the deformation driving forces at both large and small scales. There is no doubt that deformation is primarily driven by boundary forces associated with plate motion (Elliott & Freymueller, 2020; Elliott

et al., 2010, 2013; Enkelmann et al., 2017; Finzel et al., 2014; Mazzotti & Hyndman, 2002; McKay et al., 2021; Richardson & Reding, 1991; Wdowinski, 1998; Zoback, 1992b), buoyancy/body forces (Finzel et al., 2014; Mazzotti & Hyndman, 2002), and traction at the base of the lithosphere due to mantle drag (Bokelmann, 2002; Bolton et al., 2021; Finzel et al., 2011, 2014; Forte et al., 2010; Gough, 1984; McConeghy et al., 2022; Schutt et al., 2023). However, none of these mechanisms alone is sufficient to drive all of the deformation observed in the area (Heidbach et al., 2007). Quantifying their individual contributions to the stress (tensor) field is challenging and their relative roles in influencing the deformation field remain largely speculative. Each of these drivers implies a characteristic orientation of the resulting deviatoric stresses, which can be compared with the observed stress field inferred from earthquake focal mechanisms (Arnold & Townend, 2007; Gephart & Forsyth, 1984; Townend et al., 2012), seismic anisotropy (Savage et al., 2016), or borehole breakout data (Zoback & Mooney, 2003). However, the present-day stress fields of the entire orogen have only been studied at local scales, such as in Alaska (Estabrook & Jacob, 1991; Ruppert, 2008), the Mackenzie Mountains (Gough et al., 1983), the northern slope of the Brooks Range (Dixit et al., 2017), the Alberta foreland basin (Bell & Gough, 1979; Gough & Bell, 1981; Reiter et al., 2014), the Queen Charlotte Fault (Ristau et al., 2007), and the Cascadia subduction zone (Balfour et al., 2011).

We take a large-scale approach to quantify the individual stress field contributions of plate boundary forces, gravitational potential energy (GPE) variations within the lithosphere (buoyancy forces), and basal tractions by comparing modeled stress trajectories with a compilation of the observed crustal stress field. This scale of analysis requires accounting for the spherical geometry of stress fields. Using a novel statistical technique for spherical stress data proposed by Wdowinski (1998) and recently improved by Stephan et al. (2023), we model the direction of the plate boundary stresses from relative plate motion, estimate the GPE variations using topography and crustal densities, and infer the direction of basal tractions from the seismic anisotropy in the upper mantle. This study therefore represents the first large-scale, quantitative statistical analysis for the region, directly comparing the orientation of observed stress with modeled first-order stresses from these potential driving forces to evaluate their spatially resolved relative contributions to the crustal stress field. The presence of multiple stress provinces and tectonic interactions makes region ideal for studying the complexities of stress partitioning and deformation.

2. Tectonic Background

Present day seismic activity is mainly concentrated along the active plate boundaries along the western margin of North America. Alaska is primarily affected by the subduction of the Pacific plate beneath the North American plate, both of which converge at the Aleutian plate boundary at rates between 56 and 79 mm yr^{-1} (Global Strain Rate Model, GSRM, v2.1; Kreemer et al., 2014). The northward-moving Yakutat microplate (64–72 mm yr^{-1}, Elliott et al., 2010), a buoyant and overthickenned oceanic plateau (Christeson et al., 2010), causes flat-slab subduction beneath south-central Alaska and seismicity reaching far north of the Denali Fault (Figure 1). In coastal southeast Alaska and southwest Yukon, the Yakutat collision causes very rapid rock exhumation rates (Enkelmann et al., 2009, 2015) that is interpreted to related to transpression (Freymueller et al., 2008; Haeussler, 2008). The Yakutat/North American plate boundary transitions from the transpressional Fairweather Transform to the south to the St. Elias Fold-and-Thrust Belt to the north—a distributed contractional zone extending from southwestern Yukon to the Copper River. The geodetic velocity field indicates westward and eastward rotation of the surface motions away from the Yakutat collision zone (i.e., Chugach–Saint Elias Mountains). These displacements of fault-bounded fragments of the North American lithosphere are interpreted as lateral escape movements away from the major collision zone, producing margin-parallel motion along the Aleutian Arc and the Queen Charlotte Fault to the west and the east of the collisional zone, respectively (Elliott & Freymueller, 2020; Elliott et al., 2010, 2013). Recent earthquake relocations in southwest Yukon reveal a corridor of clockwise-rotating blocks situated between the eastern Denali Fault and the Connector Fault, that connects the Fairweather Transform with the Totshunda and central Denali Fault across the St. Elias Mountains (Biegel et al., 2024). Seismicity along the eastern Denali Fault is generally sparse; instead compression is accommodated by regional thrusts that crosscut the eastern Denali Fault.

Farther south, seismicity is mostly concentrated offshore along the dextral transpressive Queen Charlotte Transform, which accommodates motion between the Pacific and North American plates. Here, seismicity
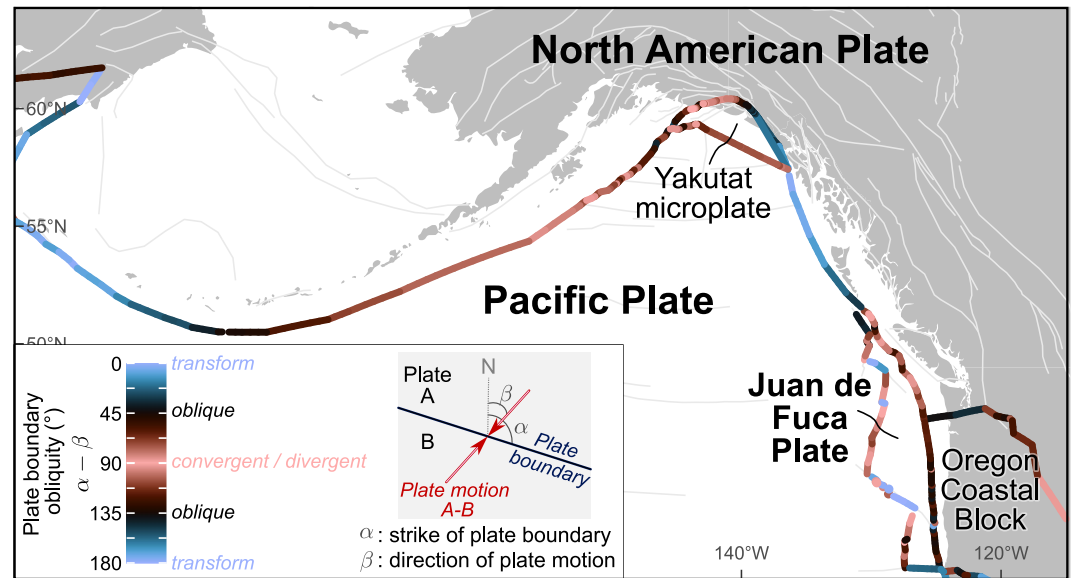
Figure 2. Plate-boundary obliquity, that is, the angle between the relative plate motion (GSRM v2.1, Table 1) and the strike of the plate boundary (Bird, 2003). Slip partitioning, or distributed transpression or transtension are expected at oblique plate boundaries.

reaches magnitudes of up to 8.1 (Haida Gwaii 1949, Hyndman, 2015). In the southern Canadian Cordillera, deformation is instead attributed to the subduction of the Juan de Fuca Plate beneath North America. Along the Cascadia Trench, convergence reaches rates up to 38–50 mm yr^{-1} (Figure 1) and is perpendicular in the north and oblique (45°) along the southern segments of the Cascadia Trench (Figure 2). Geodetic evidence indicate that the plate boundary is currently locked, causing elastic strain to build up in overriding North American Plate (McCaffrey et al., 2000). GPS data further show that crustal fragments of North America move northward and trench-parallel at rates of 23–28 mm yr^{-1} with respect to the stable plate's interior (McCaffrey et al., 2013), suggesting fragmentation of the plate into several tectonic blocks such as the Oregon Coastal Block and the Sierran Block (Lewis et al., 2003; Unruh & Humphrey, 2017; Wells et al., 1998). This fragmentation is interpreted to be driven by Basin-and-Range extension in the southeast and the oblique convergence at the Cascadia Trench (Humphreys & Hemphill-Haley, 1996).

Far-field seismicity also occurs inboard of the active plate boundaries, particularly in the north, along the northern slope of the Brooks Range, the Richardson Mountains, and the Mackenzie Mountains (Figure 1a). The largest event recorded in these regions is the 1985 M_w 6.9 earthquake in the Mackenzie Mountains. GPS data indicate a general NE directed surface motion (Leonard et al., 2007). In contrast, the Rocky Mountains farther south are seismically inactive today. Borehole breakouts from the Alberta Basin, within the eastern foreland of the Rocky Mountains, reveal a present-day NE–SW compressional stress field, orientated approximately perpendicular to the mountain belt (Reiter et al., 2014).

3. Data and Analysis

We compiled present-day stress data (n = 5452, Figure 1b) from the World Stress Map database (Heidbach et al., 2025) and literature (Balfour et al., 2011; Levandowski et al., 2018; Lund Snee & Zoback, 2020). The compilation includes only A–D quality ranked data, that is, data with an azimuth accuracy of <40° (Zoback, 1992a). Lateral limits of the stress subset and the investigated area are the westernmost Aleutians and the southernmost extent of the Juan de Fuca plate. For statistical comparisons to other fields, the measured stress orientations are quality-weighted by the reciprocal of the reported standard deviation of the azimuths.

We compare the orientation of the compiled, observed stress field (Figure 1b) with those of the fields of potential stress sources including (a) plate boundary forces (Figure 3), (b) the upper mantle drag at the base of the lithosphere (Figure S2a in Supporting Information S1), (c) body forces induced by gravitation (Figure S2b in Supporting Information S1), and the (d) the surface deformation (Figure S2c in Supporting Information S1).
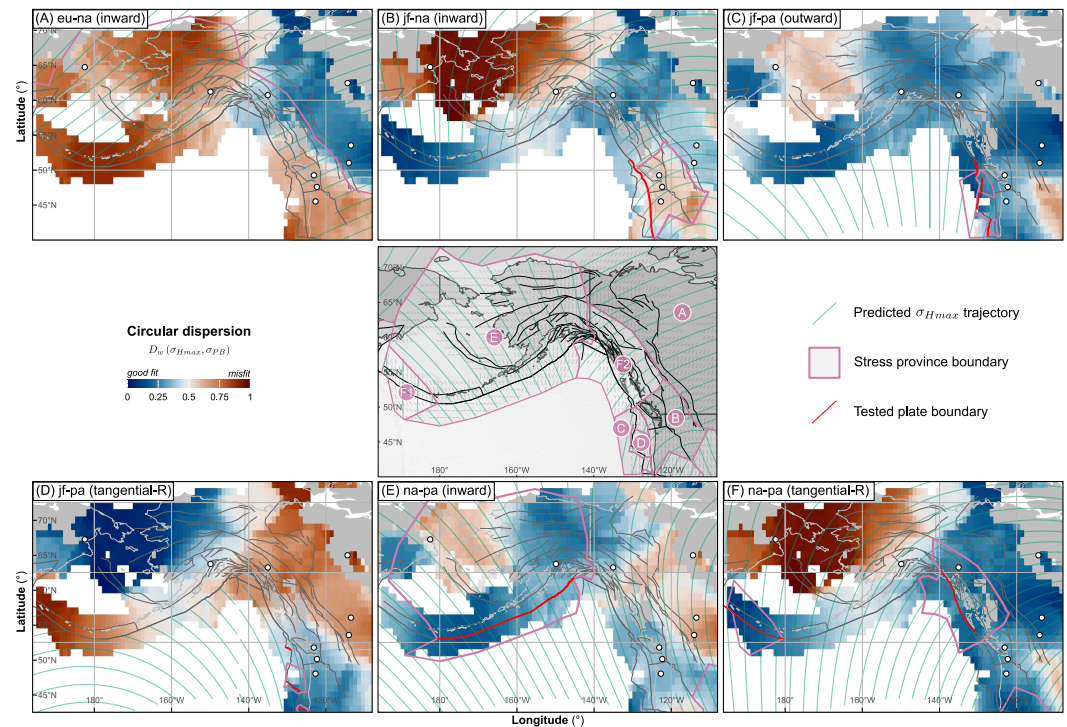
Figure 3. (a–f) Kernel dispersion showing regional deviations of the orientation of plate boundary stresses from the observed maximum horizontal stress directions (σ_{Hmax}). Blue and red colors indicate a good-fit or systematic misfit between the two directions, respectively. Red lines show the tested plate boundary. Adaptive kernel half-widths range between 100 and 50 km. Figure in center shows stress province model with labels referring to best-fit areas determined by the kernel dispersion shown subfigures (a–f). For description of abbreviated relative plate motions and statistical summaries see Table 2.

Additionally, we investigate the influence of the Yakutat microplate and the Oregon Coastal Block on the stress fields as shown in detail in Supporting Information S1 (Text S6). Data and modeling procedure are described below, while details for the modeled direction of basal drag are given in Text S5 in Supporting Information S1.

The diffuse plate boundary zone involves four neighboring plates (i.e., North America, Pacific Plate, Juan de Fuca Plate, and Eurasia) with six different plate boundary segments (Figure 3). To analyze their effects, we first subdivide the study area into subsets of different stress fields based on the lateral misfit of the modeled plate boundary stresses. These stress provinces are then compared with modeled fields of other potential sources to evaluate their local contribution to deformation.

For a statistical evaluation (e.g., variance and mean) and comparison of stress fields, orientation data must be transformed in a common reference frame. The commonly used geographical reference frame, where orientations are measured as deviations from geographic North, is unsuitable for such statistical treatment because the angles are distorted by Earth's spherical geometry (Stephan et al., 2023). Since plate boundary forces are the dominant source for the first-order stress field (Heidbach et al., 2007; Zoback et al., 1989), their stress trajectories provide an ideal reference frame for stress field analysis (see details below). All transformed stress and strain fields are then interpolated onto a common $1 \times 1°$ grid spanning the study area as shown in Figure 1. The interpolation uses an inverse distance-weighting method, described in Text S2 (Supporting Information S1). The goodness-of-fit of stress models is quantified using circular statistical metrics, such as the angular distance and the circular dispersion (see Text S1 in Supporting Information S1 for mathematical formulations). Residuals between modeled and observed stress orientations, that is, the angular distances, are interpreted as stress anomalies, that is, regions where the observed stress field deviates that expected from a tectonic force. Details on data sources and analytics are provided below.

Table 1
Parameters for Considered Relative Plate Motions

Moving plate/block	Lat. (°N)	Lon. (°E)	Rate (°Myr^{-1})	Source
with respect to North America (na)				
Eurasia (eu)	70.73	121.11	0.227	calc. from GSRM 2.1
Juan de Fuca (jf)	32.28	−112.74	−1.133	calc. from GSRM 2.1
Oregon Coastal Block (ocb)	45.16	−190.01	−1.019	McCaffrey et al. (2007)
Pacific (pa)	49.33	−76.13	−0.791	GSRM 2.1
Yakutat (yk)	59.47	−87.82	−1.04	Elliott et al. (2010)
with respect to Pacific				
Juan de Fuca	−0.73	97.50	0.625	calc. from jf-na and pa-na
Yakutat	−70.38	14.68	−0.315	yk-na and pa-na
with respect to Oregon Coastal Block				
Juan de Fuca	24.81	84.60	0.28	calc. from ocb-na and jf-na

Note. Rate is positive for counterclockwise rotation.

3.1. Directions of Plate Boundary Stresses

To model the directions of these plate boundary stresses (σ_{PB}), we use the methodology by Wdowinski (1998), that has been recently updated by Stephan et al. (2023). The method uses the empirical link between the direction of relative plate motion and the first-order orientation of the maximum horizontal stress (σ_{Hmax}) adjacent to the plate boundary. The first-order direction of σ_{Hmax} is parallel to the orientation of lateral plate boundary stresses (Heidbach et al., 2007), which are at a specified angle to trajectories of the relative motion of neighboring plates (Forsyth & Uyeda, 1975). According to the empirical model by Wdowinski (1998), the angle depends on the direction of displacement of the plate boundary, that is, σ_{Hmax} is parallel, perpendicular, or $\pm 45°$ to the direction of relative plate motion at a plate boundary that is displaced inward (convergent plate boundaries and ridge-push), outward (divergent plate boundary), or tangential (transform boundary), respectively (Figure 1b).

The predicted orientations of tested plate boundary stresses for each datapoint are obtained by transforming the coordinates and the azimuth of the stress field into a coordinate reference frame of the relative plate motion in which coordinates and azimuths are measured from the pole of rotation as the coordinate origin (Stephan et al., 2023; Wdowinski, 1998). This plate boundary stress reference frame then allows us to statistically compare the directions of plate boundary stresses with the observed directions of σ_{Hmax}. A statistically significant correlation between the (transformed) σ'_{Hmax} and the modeled direction of lateral plate boundary stresses σ_{PB} (i.e., direction of σ'_{PB} is 0° for outward, 45° for left-lateral tangential, 90° for inward, and 135° for right-lateral tangential displacement) exists when the σ'_{Hmax} orientations are normally distributed around the orientation of σ'_{PB}.

The required plate motion parameters to model the direction of σ_{PB} and transform the direction of σ_{Hmax} are derived from the GSRM v2.1 model (Kreemer et al., 2014). Block motions of Yakutat and the Oregon Coastal Block are derived from Elliott et al. (2010) and McCaffrey et al. (2007), respectively. We chose these plate motion models because they incorporate only GPS/GNSS-derived velocities and no earthquake slip. Thereby, we avoid circularity when comparing plate motion to stress field data that are partially derived from earthquake slip inversion. To obtain the relative motions, we converted all rotations into rotations relative to the North American and Pacific plates using transformation as described in Schaeben et al. (2021, 2024). The relative plate motion parameters are given in Table 1. For statistical comparisons, the modeled directions are weighted by the inverse of the potential error of the pole of rotation, which is proportional to the distance of the pole to the stress data (Stephan et al., 2023). These errors are listed in Table 2.

3.2. Direction of Gravitation-Induced Body Forces

To explore the effect of gravitation, we calculate the GPE from the topography and the crustal structure and derive the magnitudes and orientation of the gravitational deviatoric stresses based on the method by Flesch et al. (2001). Moho depth and crustal densities are derived from CRUST1.0 model (Laske et al., 2012), and the topography is

Table 2
Statistical Parameters and Test Results for the Stress Provinces

Stress province	Plate boundary[a]	n	Variance[c]	Observed azimuth Quasi-median (°)[c]	Mean (°)[c]	95% CI (°)	Predicted azimuth (°)[b]	Dispersion[c,d]	Rayleigh test[e]
Eurasia wrt. North America (eu-na)									
(A)	inward	665	0.32	71	72	63–83	90 ± 1	0.23 ± 0.02	20.03 (1e−87)
Juan de Fuca wrt. North America (jf-na)									
(B)	inward	1662	0.47	44	57	35–52	90 ± 1	0.51 ± 0.02	−1.32 (0.91)
	tan (L)						45 ± 1	0.23 ± 0.02	30.69 (2e−204)
	tan (R)						135 ± 1	0.77 ± 0.02	−30.69 (1)
Juan de Fuca wrt. Pacific (jf-pa)									
(C)	outward	132	0.16	155	160	148–171	180 ± 1	0.19 ± 0.01	10.29 (3e−24)
(D)	tan (R)	97	0.17	116	118	104–132	135 ± 1	0.16 ± 0.03	9.47 (9e−21)
North America wrt. Pacific (na-pa)									
(E)	inward	1869	0.48	96	92	86–199	90 ± 1	0.25 ± 0.01	31.76 (5e−219)
(F1-2)	tan (R)	609	0.33	124	126	118–134	135 ± 1	0.18 ± 0.02	22.35 (2e−108)

Note. Azimuths are given in transformed orientations with respect to the pole of rotation. Note that stress province (B) is tested against three different plate boundaries. Location of stress provinces shown in Figure 3. See Text S1 in Supporting Information S1 for details on statistics of angular data. CI—confidence interval, n—number of data. [a]Tangential (tan) plate boundaries are either right (R) or left (L) lateral. [b]Azimuth ± standard error. Error is estimated from Stephan et al. (2023), Equation 18. [c]Weighted by reciprocal of reported uncertainties. Quasi-Median (on the circle) after Ratanaruamkarn et al. (2009). [d]Circular dispersion ± standard deviation (bootstrap estimate of 1000 resamples). Values range from 0 (statistical fit) to 1 (systematic misfit). Weighted by reciprocal of reported uncertainties. [e]Statistical test for circular uniform distribution with specified mean direction (i.e., predicted azimuth): test statistic (*p*-value). The Null Hypothesis is rejected if the test statistic is ≥ *p*-value.

from the ETOPO1 model (NOAA National Geophysical Data Center, 2009). Because GPE distribution calculated for a lithosphere not fully compensated would produce the same overall pattern of deviatoric stress (Finzel et al., 2014; Flesch & Kreemer, 2010), we calculate the estimates of GPE distributions to a depth of 100 km for the area and model the direction of the maximum horizontal stress induced by gravitation (i.e., the horizontal gradient of GPE field) within the 1 × 1° grid as used for the plate boundary stresses. For the GPE estimate, we assume a constant mantle density at Moho depths of 3.32 g cm^{-3} (the mean mantle density of the CRUST1.0 model for the investigated area). The calculations are performed using the MATLAB program "`stress-modelling`" (Hirschberg et al., 2019). The magnitudes of the modeled GPE stresses are used as weighting coefficients for statistical estimations and comparisons.

3.3. Direction of Horizontal Principal Strain Axes

For a first-order approximation of the surface deformation, we use the horizontal strain rate tensor field that is deduced from surface GNSS velocities. Geodetic strain rates and the orientations of the horizontal principal strain axes are derived from GSRM v2.1 (Kreemer et al., 2014). To allow the comparison with other fields, we downscaled the data sets's original 0.3 × 0.3° resolution to a 1 × 1° resolution that is the same grid as used for the plate boundary stresses. The downscaling has been done by averaging the geodetic horizontal shortening directions $(\dot{e}_3)$ using the spatial interpolation algorithm as described in Supporting Information S1. The geodetic velocity is used as weighting coefficient for statistical estimations and tests.

3.4. Statistical Measure of Misfit

To evaluate the misfit between the directions of the observed and the modeled stress fields (plate boundary stresses, stresses generated by the horizontal gradient of gravitation-induced body forces, and stresses resulting from basal tractions), we use the circular dispersion (*D*). This criterion measures the sample-size normalized spread of directions around a specified orientation with values ranging from 0 to 1. Low values ($D < 0.25$) indicate a statistical alignment whereas large values ($D > 0.4$) represent a systematic misfit. The mathematical formulations of the (weighted) circular dispersion is given in Text S1 in Supporting Information S1.
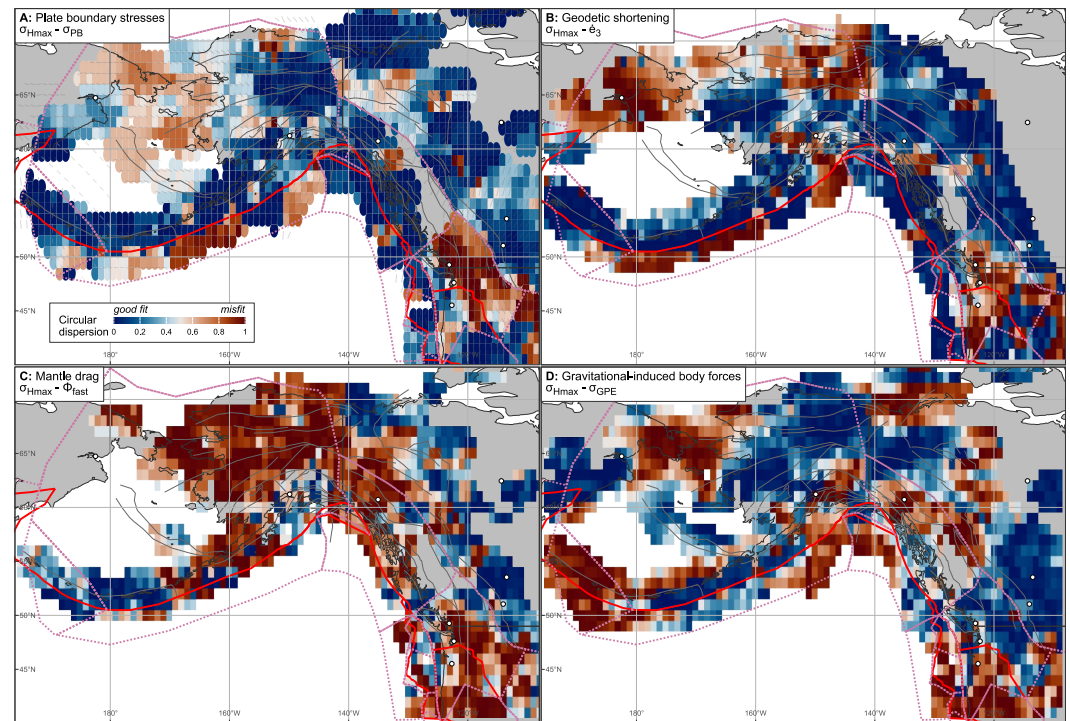
Figure 4. Misfit of tested deformation fields to the observed crustal stress (σ_{Hmax}). (a) Plate-boundary forces (represented by modeled maximum horizontal stress σ_{PB}). (b) Surface strain (represented by direction of principal shortening axes $\dot{e}_3$). (c) Mantle anisotropy (represented by slowest directions of seismic anisotropy ϕ_{slow}). (d) GPE-induced maximum horizontal stress σ_{GPE}. Pink dashed lines show the 10 Stress provinces (Figure 3, Table 3).

Because the study area contains multiple plate boundaries (Figure 1) with different displacement types, (i.e., different predicted azimuths of plate boundary stresses), we use statistical parameters to divide the study area into stress provinces that delineate areas of uniform stress fields relative to a predicted direction of plate boundary stresses. A stress province must meet the following criteria: (a) small circular dispersion ($D \leq 0.25$, i.e., "average" deviation $\leq 30°$), (b) the direction of σ'_{PB} is captured by the estimated confidence interval of the direction of σ_{Hmax}, (c) the direction of σ_{Hmax} is circular uniformly distributed around the direction of σ'_{PB} (using the Rayleigh test, e. g., Mardia & Jupp, 2000), and (d) the circular variance $Var(\sigma_{Hmax})$, is explained solely by the dispersion around the predicted σ'_{PB} azimuth, that is, $D(\sigma'_{Hmax}, \sigma'_{PB}) \sim Var(\sigma_{Hmax})$. The spatial extent of a province is determined by the lateral circular dispersion for all predicted azimuths resulting from neighboring plate boundaries (Figure 3). This kernel dispersion calculates the inverse-distance and quality weighted dispersion within a specified radius (see Text S3 in Supporting Information S1 for details).

4. Results and Discussion

4.1. First-Order Driver of Deformation in the Cordillera

Our geometric and statistical analysis of the stress field of the Canadian Cordillera and Alaska reveals seven distinct provinces, each of which is dominated by a different plate boundary force (Figure 3, statistical estimators and test results are presented in Table 2). The analysis corroborates that plate boundary forces are the dominant primary driver of deformation in the diffuse plate boundary zone of Alaska and the Canadian Cordillera (Figure 4a). Depending on the orientation of the plate boundary, the stress field is statistically best aligned with forces resulting from either convergent or transform motion of the Pacific Plate relative to North America. In the north and the east, the direction of the observed stresses across the Aleutian and the Queen Charlotte Transform are aligned with expected directions caused by convergence or transform motions, respectively ($D = 0.25$ for convergent and $D = 0.18$ for dextral transform plate boundaries between the North American and the Pacific plates, Table 2). The analysis also reveals marginally better fits for the stress fields across the convergent and dextral transform plate boundaries between Yakutat and North America ($D = 0.22$, and $D = 0.11$, respectively;

details given in Text S6, Table S1, and Figure S5 in Supporting Information S1). Thus, the Yalkutat microplate only exerts a second-order influence on a far-inboard reaching stress field that is primarily controlled by subduction and collision resulting from the Pacific-North America interactions (Estabrook et al., 1988; Page et al., 1995).

4.2. Plate Boundary Obliquity and Slip Partitioning

Several plate boundaries are notably oblique with respect to relative plate motion in the study area, in particular along segments of the Pacific-North American plate boundary (Figure 2). Such oblique plate boundary geometries give rise to slip partitioning, which is the separation of the oblique slip vector into plate margin normal and parallel components. This means that, at convergent plate boundaries, slip partitioning results in contraction and, thus, thrusting with σ_{Hmax} perpendicular to the plate boundary and localized strike-slip with σ_{Hmax} parallel to plate motion more distant from the boundary. As the stress field is tested against the dominant displacement type of the plate boundary, slip partitioning produces a significant stress deviation.

4.2.1. Bending of the Aleutian Arc

In the westernmost and easternmost Aleutian Arc, the convergent boundary between the North American and the Pacific plates becomes parallel to the relative plate motion, thus changing the displacement character to a dextral and sinistral transform plate boundary, respectively (Figure 2). While the transform tractions source the stress field in the westernmost Aleutians, southeast Alaska and coastal British Columbia, the oblique segments between the convergent and transform boundaries cause the slip to partition into thrust and strike-slip domains (e.g., Tikoff & Teyssier, 1994). For example, along the oblique segment of the Western Aleutians, observed stress orientations slightly deviate from orientations expected for both a convergent and transform boundary (Figures 3e, 3f, and 4a). Thereby, strike-slip faulting accommodating transform motions is restricted along a narrow, margin-parallel fault zone, namely the Bering Fault Zone (Figure 1; Ekström & Engdahl, 1989; Cross & Freymueller, 2008). Similar to the Great Sumatran Fault along the oblique Sunda Trench (e.g., Fitch, 1972; McCaffrey, 1992, 1996), the Bering Fault Zone accommodates the majority of transform motion of the western Aleutian Bend in the upper North American Plate, where the Pacific Plate subducts obliquely beneath the Aleutian Arc (Figure 2). Furthermore, the location of active arc volcanism in both areas is spatially restricted to such intra-arc strike-slip faults since magma ascent is favored by transtensional step-overs along such faults (Bellier & Zoback, 1995; De Saint Blanquat et al., 1998; Rosenau et al., 2006; Schütt & Whipp, 2020).

4.2.2. Fairweather Fault and Queen Charlotte Transform

The Queen Charlotte Transform accommodates dextral transform motion between the Pacific and North American plates. Along the oblique boundary between the Yakutat microplate and the North American Plate (Figure 2), stress orientations deviate from expected plate boundary stress orientations, similar to observations in the western Aleutians (Figures 3e, 3f, and 4a). In this region, slip in a 100 km wide corridor east of the dextral Fairweather Fault and its northward extension (Connector Fault) partitions into a network of reverse and strike-slip faults that delineate rotating crustal fragments (Biegel et al., 2024). In addition, the historic Yakutat Bay earthquakes M_w 8.1 and M_w 8.2 in 1899 (not included in the World Stress Map data compilation) record geological and geomorphological evidence for reverse faulting along the Fairweather Fault in the Yakutat foothills (Plafker & Thatcher, 2013). In contrast, younger seismic events (e.g., 1958 M_w 7.9 Lituya Bay; Doser, 2010) are included in our stress compilation and record dominant strike-slip motion along the Fairweather (Figure S3 in Supporting Information S1). This indicates the widespread extent of slip-partitioning along the Fairweather Fault, but also highlights the inherent time bias in the stress or geodetic strain record, as slip partitioning can only be identified when the earthquakes accommodating the different slip components have occurred.

Most of the observed stress along the Queen Charlotte Transform (North American-Pacific plate boundary) is statistically consistent with the predicted trend of stress caused by dextral transform motion ($D = 0.18$, Table 2). Minor deviations especially normal and reverse faulting, occur along the more southern parts of the Queen Charlotte Transform associated with larger magnitude earthquakes (south of Haida Gwaii; Figure 1). Here, the plate boundary is more oblique (Figure 2) and thus forms restraining and releasing bend causing local transpression and transtension, respectively (Hyndman, 2015). Ristau et al. (2007) argued that large earthquakes along

the southern Queen Charlotte Transform result from higher shear strength due to the high angle of σ_{Hmax} to the fault. However, similar to the Fairweather Fault, large earthquakes ($M_w \geq 7$, Figure S3 in Supporting Information S1) record different σ_{Hmax} directions compared to those from smaller earthquakes in close vicinity. Because such a transient stress rotations also occur in Central Alaska along the Denali Fault (Bemis et al., 2015), the Brooks Range (Fletcher & Christensen, 1996; Stauder, 1960), and other areas (see review by Hardebeck & Okada, 2018), it underlines the bias in the stress and strain record in which larger seismic events temporarily accommodate contrasting slip components especially in oblique settings (Figure S3 in Supporting Information S1).

4.3. Far-Field Effect of Arctic/North Atlantic Ridge-Push

The alignment of the observed stress field with the modeled stresses emanating from the Pacific-Yakutat plate boundaries decreases abruptly east of the Kaltag-Tintina Fault-Rocky Mountain Trench (Figure 3). Beyond this structure, the stress orientations in the Eastern Canadian Cordillera and the foreland yield the best statistical fit with the expected directions of the Arctic/North Atlantic ridge-push. This interpretation corroborates elastic finite element modeling, which suggests that the magnitude of the ridge-push is large enough to transmit stresses across the entire North American Plate (Richardson & Reding, 1991). In addition, ridge-push as a driving force for deformation along the eastern flank of the Cordillera supports low-temperature thermochronology data from the Mackenzie and Richardson mountains (Enkelmann et al., 2019; McKay et al., 2021). These studies correlate phases of intense thrusting and erosion in the Paleogene to Miocene to changes in North America's plate motion caused by the North Atlantic opening.

4.4. Significance of the Tintina Fault in Cordilleran Stress Field

As plate boundary zones localize strain at the edges of rigid plates, transitions between the dominant stresses emanating from opposing plate boundaries occur either within or near the inboard edge of the deforming plate boundary zone. In the Andes for example, collisional and subduction-related stresses from the Nazca-South America plate boundary dominate the western flanks of the Andes, while ridge-push stresses from the South Atlantic spreading controls the eastern flanks all the way to the Nubian (West African) plate boundary in the South Atlantic (Assumpção, 1992; Assumpção et al., 2016; Wdowinski, 1998).

Our stress analysis of the Cordilleran orogen shows that the Tintina Fault and northern Rocky Mountain Trench marks the boundary of an intraplate stress province in Northern America. This lithospheric-scale structure co-incides with the western margin of the North American Craton (e.g., Busby et al., 2023; Estève et al., 2020, 2021; Gabrielse et al., 2006; Monger & Gibson, 2019; Price & Carmichael, 1986). It separates regions dominated by stresses emanating from North America's western plate boundaries from those controlled by its eastern boundary. In contrast, nearby faults that run parallel, including the Denali Fault, do not show a deflection of far-field stresses. This suggests that the structural inheritance along the Tintina Fault and the northern Rocky Mountain Trench has played a major role on shaping both present-day and past stress fields in the Cordillera, influencing its evolution since at least the Eocene (e.g., Finley et al., 2025; Padgett et al., 2025).

4.5. Why Are the Mackenzie Mountains Active Today, But Not the Rocky Mountains?

The Canadian Rocky Mountains form the eastern margin of the Canadian Cordillera, stretching >1500 km from the Yukon–British Columbia border into Montana (Figure 1). Foreland folding and thrusting ceased in the early Eocene (Pana & van der Pluijm, 2015), and the region is today seismically quiet. In contrast, the >1300 km long Mackenzie and Richardson mountains—the eastern margin of the Northern Canadian Cordillera—are still tectonically active (Figure 1a) (Cassidy & Bent, 1993; Leonard et al., 2007; Mazzotti & Hyndman, 2002). Variations in crustal strength alone do not explain the observed spatial and temporal distribution of strain.

Stress orientation along the strike of the Kaltag-Tintina Fault and the Rocky Mountain Trench structure indicate that a change in stress source is either sudden (e.g., for the southern Rocky Mountain Trench, Figures 3a and 3b) or gradual (e.g., for the northern Rocky Mountains Trench, the Tintina Fault, and the Mackenzie Mountains, Figures 3a, 3b, 3e, and 3f). Such gradual transitions suggest that multiple stress sources may superimpose and control the σ_{Hmax} orientations.
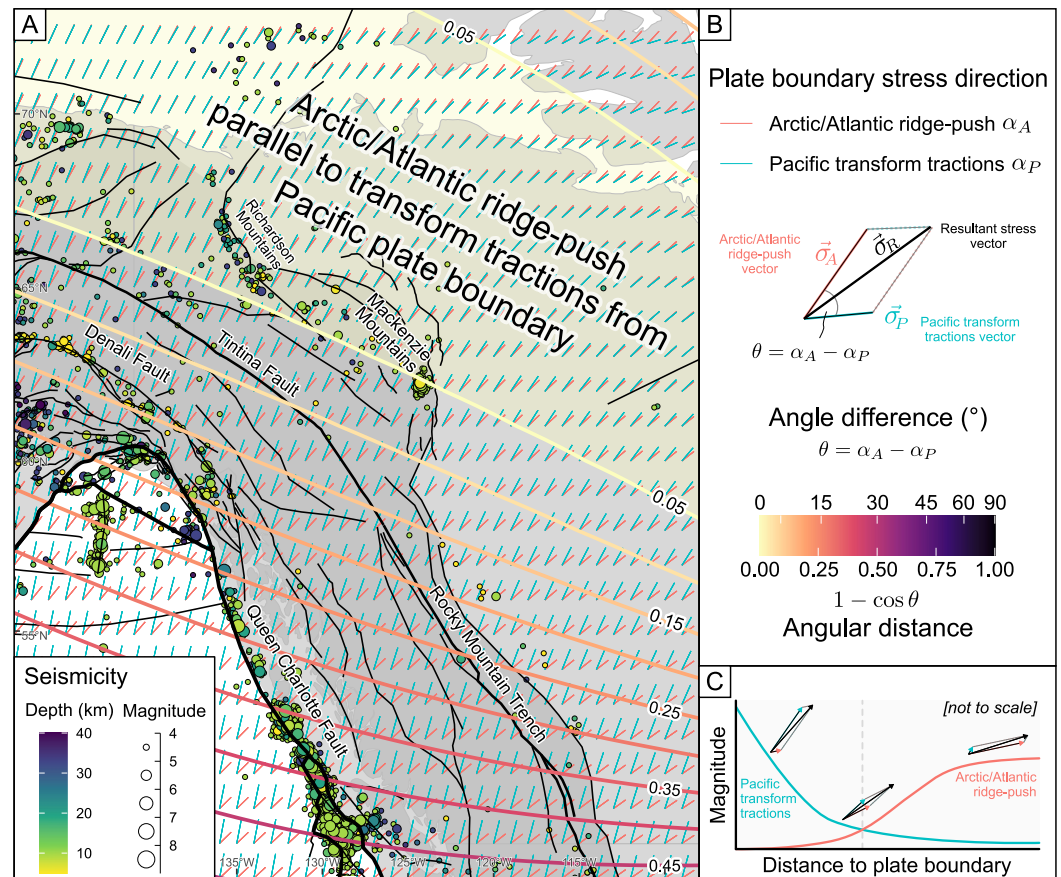
Figure 5. (a) Link between the far-field seismicity and the angles between stresses generated by Arctic/North Atlantic ridge-push and transform tractions emanating from the Pacific plate boundary. Isogons are lines of constant angles (expressed by the angular distance) between the two superimposing stresses. Blue and red bars show the directions of the Pacific and the Arctic/North Atlantic plate boundary stresses, respectively. Crustal seismicity gives the epicenters for earthquakes between 15 and 40 km depth and $M_w > 4$ since 1970 (ANSS catalog). (b) Vector parallelogram explaining the geometric relation (in terms of orientation and magnitude) between two superimposing stresses and their resultant stress. (c) Link between the magnitude of maximum horizontal stress and the distance to a plate boundary. Graphs show the variations of the resultant maximum horizontal stress due to both orientation and magnitude of the superimposing plate boundary stresses (not to scale). See Text S4 in Supporting Information S1 for details.

4.5.1. Superposition of Plate Boundary Stresses

Intraplate deformation occurs when deviatoric stresses are large enough to deform the lithosphere. This can be the result of an increase in the magnitude of a stress source (force) and/or the superposition of multiple stresses (e.g., Heidbach et al., 2007; Zoback, 1992a). Assuming that plate boundary compression is uniaxial ($\sigma_2 = \sigma_3 = 0$), the net σ_{Hmax} resulting from superposition approximates the vector sum of stresses acting on the same body (Figure 5a). As lithostatic stresses do not influence the direction of σ_{Hmax}, magnitude and orientation of the resultant σ_{Hmax} depend solely on the relative magnitude and the angle between the superimposing plate boundary stresses. Although it is beyond the scope of our study to infer local stress magnitudes from adjacent plate boundaries, the total deviatoric stress is largest when the directions of superimposed maximum compressive stresses align, and smallest when they are perpendicular (Figure 5b).

4.5.2. Implications for the Northern Cordillera

To explore the stress superposition, we overlay the modeled stresses originating from both the western and eastern plate boundaries of North America (Figure 5). Next, we calculate the intersection isogons, that is, lines of constant angles between the trajectories of the two plate boundary stresses. The isogons highlight regions where both plate boundaries stresses align, and thus, where the overall deviatoric stress is increased (yellow shaded area in

Figure 5a). In this region, the amplification of the resultant deviatoric stresses may be large enough to reactivate existing crustal structures and trigger new deformation. Because this regions coincides with earthquake concentrations, a high deviatoric stress due to stress superposition may explain the strong seismicity of thrusting in northern Alaska, dextral strike-slip faulting in the Richardson Mountains and thrusting in the Mackenzie Mountains and Plain (Figure 5a). Farther south in the Cordillera (southern Tintina Fault and Rocky Mountain Trench), the plate boundary stresses from the western margin of North America are perpendicular to the Arctic/North Atlantic ridge push, and, thus, the reduced resultant deviatoric stress is insufficient to cause deformation.

In terms of timing, stress superposition is supported by low-temperature thermochronology revealing that post-Cordilleran deformation in the Mackenzie Mountains and Richardson Mountains (40–30 Ma) did not start before spreading initiated in the Arctic enabling ridge-push (Enkelmann et al., 2019; McKay et al., 2021). In the southern Rocky Mountains, thrusting and cooling already ceased prior to the onset of Arctic spreading, as shown by illite $^{40}Ar/^{39}Ar$ dating of thrust-fault gouges (76–72 Ma and 54–52 Ma; van der Pluijm et al. (2006); Pana and van der Pluijm (2015)) and low-temperature thermochronology (∼60 Ma; Damant et al. (2023)).

4.6. Strain Anomaly in Southern British Columbia and Washington

The seismically active coastal region of southern British Columbia and Washington State (west of the Fraser River Fault-Straight Creek Fault, Figure S4 in Supporting Information S1) is expected to be stressed by the convergence between the Juan de Fuca Plate and the North American plate. In the north, this involves orthogonal subduction of the Juan de Fuca Plate beneath the North American Plate (Figure 2), while in the south, subduction becomes highly oblique to the relative plate motion promoting slip partitioning into margin-normal thrusting and margin-parallel dextral strike-slip within the overriding North American plate. Testing the stress field against the plate kinematics of North America and the Juan de Fuca plate shows that margin-normal thrusting dominates at the northern Cascadia Trench (Figure S4 in Supporting Information S1). Stresses in the hinterland, however, are trending parallel to the plate boundary—contrary to a dextral strike-slip stress field expected from relative motions (Figure S4 in Supporting Information S1). Moreover, oblique stresses in the hinterland are not accommodated along a single discrete fault, but rather distributed across southern British Columbia and Washington State, particularly between the Cascadia Trench and the Fraser River Fault and the Yakima Fold-and-Thrust Belt (Figure S4 in Supporting Information S1). Despite the partial alignment with the trend of the active volcanic arc, the observed stress directions differ notably from those predicted from an oblique subduction zone. Comparisons with relative motions yield poor fits for:

- Pure convergence between North America and Juan de Fuca: $D = 0.51$ (Table 2),
- Pure dextral transform displacement between North America and Juan de Fuca: $D = 0.77$ (Table 2),
- Convergence between Juan de Fuca Plate and the Oregon Coastal Block: $D = 0.56$ (Table S1 in Supporting Information S1), and
- Northward push of the Oregon Coastal Block with respect to North America: $D = 0.62$ (Table S1 in Supporting Information S1).

This shows that the observed stress field is highly oblique to all predicted stress trajectories, desite the fact that the surface motions of the Oregon Coastal Block are well constrained by geodetic studies (Balfour et al., 2011; Wang, 2000), Moreover, the high angles between stress trajectories emanating from the Juan de Fuca and Oregon Coastal Block boundaries would reduce the magnitude of the resulting maximum horizontal stress (see Figure S4 in Supporting Information S1), which is in conflict with the enhanced seismicity recorded in the area (Figure 1). Gravitational-induced stresses ($D = 0.39$, Table 3) and the upper mantle anisotropy ($D = 0.33$, Table 3) also show poor alignment, suggesting these sources alone have only a minor influence on the orientation of the stress field—though a combined effect of block motions, mantle drag and GPE-induced stresses cannot be excluded by our method.

Our test reveals that the stress field in southern British Columbia and Washington is best aligned with a stresses expected for a left-lateral tangential plate boundary between the Juan de Fuca and North American plates ($D = 0.23$, Table 2). Although this suggested displacement is in conflict with the actual displacement between the two plates, it shows that stresses emanating from the oblique (dextral convergent) plate boundary are accommodated by sinistral faulting, resulting in plate-margin-parallel compression. Such a geometry supports the model by Wells et al. (2020), in which the clockwise rotation of the Cascadian forearc occurs via minor sinistral step-over or antithetic Riedel shear faults progressively rotating between major dextral faults in a domino-style

Table 3
Dispersion of Modeled Stress Directions From Observed Direction of Maximum Horizontal Stress (σ_{Hmax})

Stress province	$D(\sigma_{Hmax}, \sigma_{PB})$	$D(\sigma_{Hmax}, \dot{e}_3)$	$D(\sigma_{Hmax}, \phi_{slow})$	$D(\sigma_{Hmax}, \sigma_{GPE})$
(A) Mid-Plate (east of Rocky Mountain Trench)	0.23 ± 0.02	0.23 ± 0.02	0.61 ± 0.02	0.36 ± 0.02
(B) Southern British Columbia and Washington (Cascadia Megathrust to Rocky Mountain Trench)	0.23 ± 0.02	0.56 ± 0.05	0.33 ± 0.03	0.39 ± 0.07
(C) Pacific Ocean west of Juan de Fuca Ridge	0.19 ± 0.02	0.09 ± 0.04	0.32 ± 0.07	0.65 ± 0.06
(D) Juan de Fuca Plate	0.16 ± 0.03	0.15 ± 0.16	0.37 ± 0.10	0.80 ± 0.12
(E) Aleutian Arc, Bering Sea, Chukotka, and Alaska	0.25 ± 0.01	0.50 ± 0.03	0.33 ± 0.03	0.44 ± 0.02
(F1) western Aleutian Arc and (F2) Coastal Range (east of Queen Charlotte Fault) and SW Yukon (Fair weather Fault Zone to Tintina Fault)	0.18 ± 0.02	0.18 ± 0.02	0.40 ± 0.04	0.67 ± 0.04
Total	0.32	0.36	0.36	0.33

Note. Location of stress provinces shown in Figure 3. *D*—Dispersion, $\dot{e}_3$—azimuth of horizontal surface shortening, σ_{GPE}—stress deduced from gravitational potential energy per volume unit, σ_{PB}—azimuth of plate boundary force, ϕ_{slow}—azimuth of slow direction of seismic anisotropy. Standard deviation of the circular dispersion is a bootstrap estimate of 1,000 resamplings. Dispersion from plate boundary forces are the results shown in Table 2.

manner. This scenario places the southern Canadian Cordillera within a broader diffuse plate boundary extending from the Colorado Plateau to the Cascadian margin. Our test results thus support the concept of a large-scale transrotational domain or "bookshelf slip" system that accommodates the Pacific–North America shear by extensional strain in the Basin and Range Province and compression near and parallel the plate boundary (Atwater, 1970; Darin & Dorsey, 2013; Dickinson, 1996; Luyendyk et al., 1980; Platt & Becker, 2013).

4.7. Second-Order Drivers of Deformation

Our analysis shows that most deformation in the Cordillera can be explained by plate boundary forces and the superposition of their generated stresses. The negligible improvements in model fits for the Yakutat microplate and the significant misfits for the Oregon Coastal Block suggest that smaller plates and blocks exert only minor (second-order or less) influence on the overall stresses in the study area, since they are an integral part of the diffuse plate boundary. Some interior regions can not be explained by boundary forces and represent stress anomalies as seen in the Columbia Mountains in southeastern British Columbia and the Brooks Range in northern Alaska (red areas in Figure 4a). Such stress deviations from the trajectories of plate boundary stresses are caused by second-order forces, mainly gravitational-induced body forces, because of the better statistical fits of the observed stresses with their modeled stress orientation (blue areas in Figures 4c and 4d).

4.7.1. Stress Fields Controlled by Gravitational-Induced Body Forces

Our analyses show that in both areas the orientation of the maximum horizontal stress is aligned with gravitational-induced stresses (Figure 4d). In a compressional orogen, the excess of gravitational potential energy from crustal overthickenning leads to an increase of vertical stresses eventually exceeding the magnitude of σ_{Hmax}. The orientation of σ_{Hmax} remains aligned with the convergence direction resulting in crustal extension perpendicular to the convergence direction. This can been seen in the plateaus of Tibet in Central Asia and Altiplano in the Andes (England & Molnar, 1997; Molnar & Lyon-Caen, 1988; Molnar et al., 1998; Stephan et al., 2023). In the Brooks Range normal faulting occurs exclusively with σ_{Hmax} aligned with the convergence direction between North America and the Pacific plate (Figure 1b). This gravitational collapse with extension perpendicular to the convergence direction is supported by the direction of the principal stretching axes derived from geodetic motions (Figure S2c in Supporting Information S1).

In southeastern British Columbia and Washington state, east of the Fraser River Fault-Straight Creek Fault, the transition from transpressive to transtensive stresses implies an increase of vertical stresses, particularly between the Fraser River Fault and the southern Rocky Mountain Trench. Present-day normal faulting has not been reported indicating that vertical stresses do not exceed the magnitude of horizontal stresses. However, the extensional component of the area is supported by low-temperature thermochronology that records Oligocene and Miocene cooling due to reactivation of normal faults (Damant et al., 2023; Fraser et al., 2021). The oblique nature

of the faulting regime indicates a deviation from Andersonian style of faulting, likely caused by the reactivation of non-ideally oriented faults, enhanced by high pore-fluid pressure and/or low frictional strength (Anderson, 1905; Byerlee, 1978). Our test reveals that stresses in the southwestern Canadian Cordillera may be superimposed by Basin-and-Range tectonics generating E-W trending σ_{hmin} (N-S trending σ_{Hmax}) parallel to the Basin-and-Range extension (Parsons et al., 1998; Puskas & Smith, 2009; Waite & Smith, 2004). Nevertheless, the area encompasses Eocene metamorphic core complexes (Armstrong, 1982; Coney & Harms, 1984), with N–S trending lithospheric-scale mechanical anisotropies. Such features suggest that the region exhibits rheological weaknesses that are subjected to prolonged crustal extension due to ongoing gravitational collapse (Lee Armstrong & Ward, 1991). The diffuse extension (see modeled gravitational-induced σ_{Hmax} in Figure S2b in Supporting Information S1) may cause the oblique reactivation of NNW–SSE striking structures such as the Columbia River Fault (Figure S4 in Supporting Information S1) and, thus, the deflection of plate boundary stresses (Damant et al., 2023; Finley et al., 2022). As a potential additional driver, the dynamics of the upper mantle beneath the Yellowstone volcanic field (Wyoming) appear to exert only a local and transient influence on stress orientation, since post-seismic relaxation has caused only minor perturbations to the Basin-and-Range-dominated stress field (Waite & Smith, 2004).

4.7.2. Stress Fields Controlled by Mantle Drag

There is no clear evidence that the stress field in the Cordillera is significantly controlled by mantle-flow induced basal tractions (Text S5 in Supporting Information S1) because plate boundary stresses and gravitational stresses exhibit statistically better fits with the orientation of the observed stress field. Nevertheless, the effect of mantle drag on the crustal stress field cannot be excluded since weak alignment of observed stresses with the slow-direction of seismic anisotropies ($D = 0.36$, Table 3) may also indicate minor contributions to in situ stresses (more details in Text S5 in Supporting Information S1).

5. Conclusions

Our geometric test supports that plate boundary forces control most of the observed stress field in the Canadian Cordillera and Alaska. Seven stress provinces reveal a mosaic of compressional, extensional, and strike-slip regimes that result from interactions among the major plates (Figure 6). The complexity of the Cordilleran stress field arises from superposition of multiple plate boundary stresses and the geometry of the plate margins:

- The eastern and northern edge of the Canadian Cordillera and Alaska, respectively, are dominated by the far-field Arctic/North Atlantic ridge push. The Kaltag-Tintina Fault–Rocky Mountain Trench marks the sharp transition from Pacific to Arctic/North Atlantic stress sources (Figure 6). This intracontinental stress province boundary coincides with the western margin of the Laurentian craton, suggesting this lithospheric-scale structural inheritance significantly controls Cordilleran deformation by deflecting far-field stresses.
- Stress superposition explains regional differences in seismicity in the far-field areas (Figure 5). Aligned plate boundary stresses amplify local deviatoric stress, promoting tectonic deformation (e.g., Mackenzie Mountains), while oblique plate boundary stresses reduce deviatoric stress and suppress deformation (e.g., southern Rocky Mountains), despite similar distances (>800 km) from the Pacific plate boundary.
- Discrete slip partitioning (Figure 2) affect stress fields along the oblique segments of the western Aleutians arc and the Queen Charlotte Transform (green area in Figure 6). In contrast, along the oblique Juan de Fuca-North American plate boundary, diffuse, bookshelf-style sinistral faulting between dextral major faults results in margin-parallel compression.
- Smaller plates (e.g., the Yakutat microplate) and blocks (e.g., the Oregon Coastal Block) exert only limited control on the overall stresses.
- Second-order forces, such as gravitational collapse, mainly control the stress fields in the Brooks Range and southeastern British Columbia (pink area in Figure 6). There is no conclusive evidence that mantle drag significantly influences the orientation of the present-day stress field (Figure 4c).

Our approach helps to identify regions needing further research where observed stresses deviate from stress predictions (i.e., stress anomalies). A lithospheric-scale approach considering all possible plate interactions and their variable characters due to spherical geometry, is essential to understand crustal stresses, especially in inboard regions where forces are generally weaker and structural inheritance becomes more dominant. The findings highlight the importance of plate boundary geometry and stress superposition in the orogenic evolution
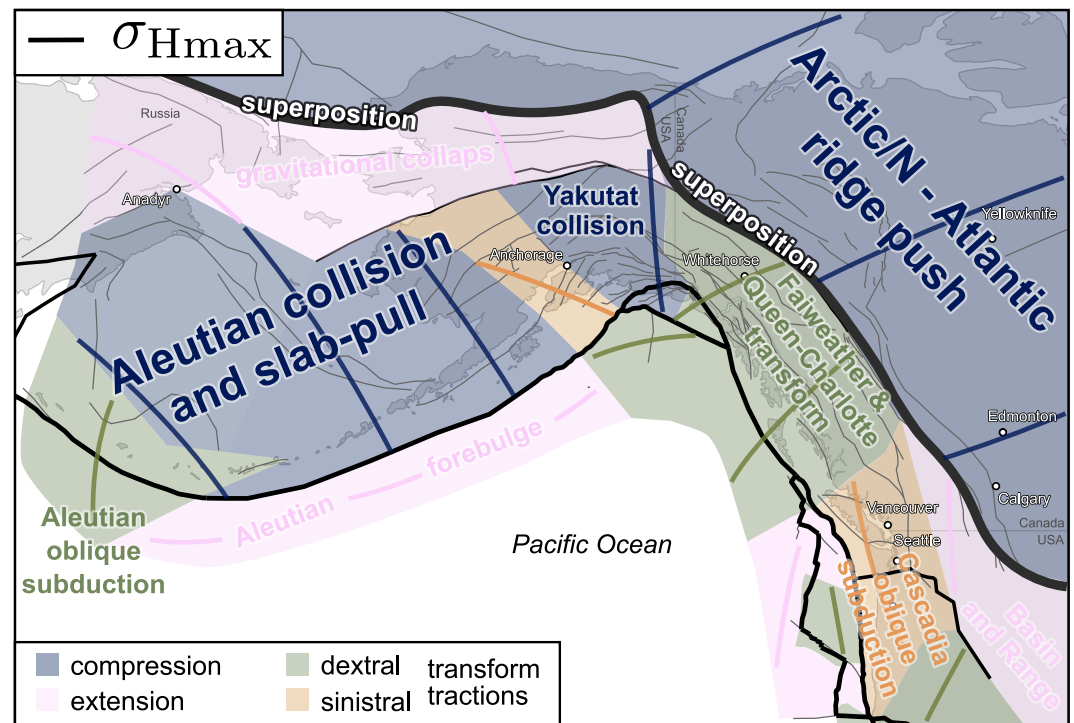
Figure 6. Stress province model for the plate boundary zone between North America and the Pacific and Juan de Fuca plates. The provinces comprise areas where the maximum horizontal stresses (σ_{Hmax}) are predominantly controlled by one plate boundary force. Colors show the different types of and kinematics of prevailing deformation.

over long time scales. As continents grow, for example, due to terrane accretion, their interior stresses evolve with changing boundary characteristics, distances, and thus magnitudes and orientation of generated stresses. Additionally, inherited lithospheric structures direct and localize intracontinental deformation where multiple plate boundary stresses align. Our method enables paleostress predictions from plate motion reconstructions, allowing a framework to integrate structural, magmatic, sedimentary, and metamorphic data to better understand the tectonic evolution of the Cordillera.

Data Availability Statement

All of the original data in this paper originate from previously published sources. The crustal stress data are from World Stress Map database (Heidbach et al., 2025) and various sources described in the section "Data and Analysis." The geodetic strain data are derived from Kreemer et al. (2014) and references therein. Moho depth and crustal densities are derived from CRUST1.0 model (Laske et al., 2012), and the topography is from the ETOPO1 model (NOAA National Geophysical Data Center, 2009). Seismic anisotropy data are compiled from Wüstefeld et al. (2009) and various sources described in the section "Data and Analysis." Statistical calculations and stress modeling were performed using the free and open-source R package `tectonicr` (Stephan, 2024).

References

Anderson, E. M. (1905). The dynamics of faulting. *Transactions of the Edinburgh Geological Society*, *8*(3), 387–402. https://doi.org/10.1144/transed.8.3.387

Armstrong, R. L. (1982). Cordilleran metamorphic core complexes—From Arizona to Southern Canada. *Annual Review of Earth and Planetary Sciences*, *10*(1), 129–154. https://doi.org/10.1146/annurev.ea.10.050182.001021

Arnold, R., & Townend, J. (2007). A Bayesian approach to estimating tectonic stress from seismological data. *Geophysical Journal International*, *170*(3), 1336–1356. https://doi.org/10.1111/j.1365-246X.2007.03485.x

Assumpção, M. (1992). The regional intraplate stress field in South America. *Journal of Geophysical Research*, *97*(B8), 11889–11903. https://doi.org/10.1029/91JB01590

Assumpção, M., Dias, F. L., Zevallos, I., & Naliboff, J. B. (2016). Intraplate stress field in South America from earthquake focal mechanisms. *Journal of South American Earth Sciences*, *71*, 278–295. https://doi.org/10.1016/J.JSAMES.2016.07.005

Atwater, T. (1970). Implications of plate tectonics for the Cenozoic tectonic evolution of Western North America. *GSA Bulletin*, *81*(12), 3513–3536. https://doi.org/10.1130/0016-7606(1970)81[3513:IOPTFT]2.0.CO;2

Balfour, N. J., Cassidy, J. F., Dosso, S. E., & Mazzotti, S. (2011). Mapping crustal stress and strain in southwest British Columbia. *Journal of Geophysical Research*, *116*(B3), 1–11. https://doi.org/10.1029/2010JB008003

Bell, J. S., & Gough, D. I. (1979). Northeast-southwest compressive stress in Alberta evidence from oil wells. *Earth and Planetary Science Letters*, *45*(2), 475–482. https://doi.org/10.1016/0012-821X(79)90146-8

Bellier, O., & Zoback, M. L. (1995). Recent state of stress change in the Walker Lane zone, western Basin and Range province, United States. *Tectonics*, *14*(3), 564–593. https://doi.org/10.1029/94tc00596

Bemis, S. P., Weldon, R. J., & Carver, G. A. (2015). Slip partitioning along a continuously curved fault: Quaternary geologic controls on Denali fault system slip partitioning, growth of the Alaska Range, and the tectonics of south-central Alaska. *Lithosphere*, *7*(3), 235–246. https://doi.org/10.1130/l352.1

Biegel, K. M., Gosselin, J. M., Dettmer, J., Colpron, M., Enkelmann, E., & Caine, J. S. (2024). Earthquake relocations delineate a discrete fault network and deformation corridor throughout Southeast Alaska and Southwest Yukon. *Tectonics*, *43*(5), e2023TC008140. https://doi.org/10.1029/2023TC008140

Bird, P. (2003). An updated digital model of plate boundaries. *Geochemistry, Geophysics, Geosystems*, *4*(3). https://doi.org/10.1029/2001GC000252

Bokelmann, G. H. R. (2002). Which forces drive North America? *Geology*, *30*(11), 1027. https://doi.org/10.1130/0091-7613(2002)030⟨1027:wfdna⟩2.0.co;2

Bolton, A. R., Schutt, D. L., Aster, R. C., Audet, P., Schaeffer, A. J., Estève, C., et al. (2021). Evidence for asthenospheric flow rotation in northwest Canada: Insights from shear wave splitting. *Geophysical Journal International*, *228*(3), 1780–1792. https://doi.org/10.1093/gji/ggab396

Busby, C. J., Pavlis, T. L., Roeske, S. M., & Tikoff, B. (2023). The North American Cordillera during the Mesozoic to Paleogene: Selected questions and controversies. In S. J. Whitmeyer, M. L. Williams, D. A. Kellet, & B. Tikoff (Eds.), *Laurentia: Turning points in the evolution of a continent* (Vol. 220, pp. 635–658). Geological Society of America. https://doi.org/10.1130/2022.1220(31)

Byerlee, J. (1978). Friction of rocks. In *Rock friction and earthquake prediction* (pp. 615–626).

Cassidy, J. F., & Bent, A. L. (1993). Source parameters of the 29 May and 5 June, 1940 Richardson Mountains, Yukon Territory, earthquakes. *Bulletin of the Seismological Society of America*, *83*(3), 636–659. https://doi.org/10.1785/BSSA0830030636

Christeson, G. L., Gulick, S. P. S., van Avendonk, H. J. A., Worthington, L. L., Reece, R. S., & Pavlis, T. L. (2010). The Yakutat terrane: Dramatic change in crustal thickness across the Transition fault, Alaska. *Geology*, *38*(10), 895–898. https://doi.org/10.1130/G31170.1

Coney, P. J., & Harms, T. A. (1984). Cordilleran metamorphic core complexes: Cenozoic extensional relics of Mesozoic compression. *Geology*, *12*(9), 550. https://doi.org/10.1130/0091-7613(1984)12⟨550:CMCCCE⟩2.0.CO;2

Cross, R. S., & Freymueller, J. T. (2008). Evidence for and implications of a Bering plate based on geodetic measurements from the Aleutians and western Alaska. *Journal of Geophysical Research*, *113*(B7). https://doi.org/10.1029/2007JB005136

Damant, K. A., Enkelmann, E., & Jess, S. (2023). Prolonged post-orogenic extension in the southeastern Canadian Cordillera: Miocene reactivation of the Columbia River Fault. *Tectonophysics*, *850*, 229763. https://doi.org/10.1016/j.tecto.2023.229763

Darin, M. H., & Dorsey, R. J. (2013). Reconciling disparate estimates of total offset on the southern San Andreas fault. *Geology*, *41*(9), 975–978. https://doi.org/10.1130/G34276.1

De Saint Blanquat, M., Tikoff, B., Teyssier, C., & Vigneresse, J. L. (1998). Transpressional kinematics and magmatic arcs. *Geological Society - Special Publications*, *135*(1), 327–340. https://doi.org/10.1144/GSL.SP.1998.135.01.21

Dickinson, W. R. (1996). Kinematics of transrotational tectonism in the California transverse ranges and its contribution to cumulative slip along the san Andreas transform fault system. *Special Papers - Geological Society of America*, *305*, 1–46. https://doi.org/10.1130/0-8137-2305-1.1

Dixit, N. C., Hanks, C. L., Wallace, W. K., Ahmadi, M., & Awoleke, O. (2017). In situ stress variations associated with regional changes in tectonic setting, northeastern Brooks Range and eastern North Slope of Alaska. *AAPG Bulletin*, *101*(3), 343–360. https://doi.org/10.1306/08051616013

Doser, D. I. (2010). A reevaluation of the 1958 fairweather, Alaska, earthquake sequence. *Bulletin of the Seismological Society of America*, *100*(4), 1792–1799. https://doi.org/10.1785/0120090343

Ekström, G., & Engdahl, E. R. (1989). Earthquake source parameters and stress distribution in the Adak Island region of the central Aleutian Islands, Alaska. *Journal of Geophysical Research*, *94*(B11), 15499–15519. https://doi.org/10.1029/JB094iB11p15499

Elliott, J. L., & Freymueller, J. T. (2020). A block model of present-day kinematics of Alaska and Western Canada. *Journal of Geophysical Research: Solid Earth*, *125*(7), e2019JB018378. https://doi.org/10.1029/2019JB018378

Elliott, J. L., Freymueller, J. T., & Larsen, C. F. (2013). Active tectonics of the St. Elias orogen, Alaska, observed with GPS measurements. *Journal of Geophysical Research: Solid Earth*, *118*(10), 5625–5642. https://doi.org/10.1002/jgrb.50341

Elliott, J. L., Larsen, C. F., Freymueller, J. T., & Motyka, R. J. (2010). Tectonic block motion and glacial isostatic adjustment in southeast Alaska and adjacent Canada constrained by GPS measurements. *Journal of Geophysical Research*, *115*(B9), 1–21. https://doi.org/10.1029/2009JB007139

England, P., & Molnar, P. (1997). Active deformation of Asia: From kinematics to dynamics. *Science*, *278*(5338), 647–650. https://doi.org/10.1126/science.278.5338.647

Enkelmann, E., Finzel, E., & Arkle, J. (2019). Deformation at the eastern margin of the Northern Canadian Cordillera: Potentially related to opening of the North Atlantic. *Terra Nova*, *31*(3), 151–158. https://doi.org/10.1111/ter.12374

Enkelmann, E., Koons, P. O., Pavlis, T. L., Hallet, B., Barker, A., Elliott, J., et al. (2015). Cooperation among tectonic and surface processes in the St. Elias Range, Earth's highest coastal mountains. *Geophysical Research Letters*, *42*(14), 5838–5846. https://doi.org/10.1002/2015gl064727

Enkelmann, E., Piestrzeniewicz, A., Falkowski, S., Stübner, K., & Ehlers, T. A. (2017). Thermochronology in southeast Alaska and southwest Yukon: Implications for North American Plate response to terrane accretion. *Earth and Planetary Science Letters*, *457*, 348–358. https://doi.org/10.1016/j.epsl.2016.10.032

Enkelmann, E., Zeitler, P. K., Pavlis, T. L., Garver, J. I., & Ridgway, K. D. (2009). Intense localized rock uplift and erosion in the St Elias orogen of Alaska. *Nature Geoscience*, *2*(5), 360–363. https://doi.org/10.1038/ngeo502

Estabrook, C. H., & Jacob, K. H. (1991). Stress indicators in Alaska. In D. B. Slemmons, E. R. Engdahl, M. D. Zoback, & D. D. Blackwell (Eds.), *Neotectonics of North America* (Vol. 1, pp. 387–399). Geological Society of America. https://doi.org/10.1130/DNAG-CSMS-NEO.387

Estabrook, C. H., Stone, D. B., & Davies, J. N. (1988). Seismotectonics of northern Alaska. *Journal of Geophysical Research*, *93*(B10), 12026–12040. https://doi.org/10.1029/JB093iB10p12026

Estève, C., Audet, P., Schaeffer, A. J., Schutt, D. L., Aster, R. C., & Cubley, J. F. (2020). Seismic evidence for craton chiseling and displacement of lithospheric mantle by the Tintina fault in the northern Canadian Cordillera. *Geology*, *48*(11), 1120–1125. https://doi.org/10.1130/G47688.1

Estève, C., Gosselin, J. M., Audet, P., Schaeffer, A. J., Schutt, D. L., & Aster, R. C. (2021). Surface-wave tomography of the Northern Canadian Cordillera using Earthquake Rayleigh Wave Group velocities. *Journal of Geophysical Research: Solid Earth*, *126*(8), e2021JB021960. https://doi.org/10.1029/2021JB021960

Finley, T., Johnston, S. T., Unsworth, M. J., Banks, J., & Pana, D.-I. (2022). Modern dextral strain controls active hydrothermal systems in the southeastern Canadian Cordillera. *GSA Bulletin*, *135*(7–8), 2015–2037. https://doi.org/10.1130/b36500.1

Finley, T., Nissen, E., Cassidy, J. F., Salomon, G., Leonard, L. J., & Froese, D. (2025). Large surface-rupturing earthquakes and a >12 kyr, open interseismic interval on the Tintina Fault, Yukon. *Geophysical Research Letters*, *52*(14), e2025GL116050. https://doi.org/10.1029/2025gl116050

Finzel, E. S., Flesch, L. M., & Ridgway, K. D. (2011). Kinematics of a diffuse North America-Pacific-Bering plate boundary in Alaska and western Canada. *Geology*, *39*(9), 835–838. https://doi.org/10.1130/G32271.1

Finzel, E. S., Flesch, L. M., & Ridgway, K. D. (2014). Present-day geodynamics of the northern North American Cordillera. *Earth and Planetary Science Letters*, *404*, 111–123. https://doi.org/10.1016/j.epsl.2014.07.024

Fitch, T. J. (1972). Plate convergence, transcurrent faults, and internal deformation adjacent to Southeast Asia and the western Pacific. *Journal of Geophysical Research*, *77*(23), 4432–4460. https://doi.org/10.1029/JB077i023p04432

Flesch, L. M., Haines, A. J., & Holt, W. E. (2001). Dynamics of the India-Eurasia collision zone. *Journal of Geophysical Research*, *106*(B8), 16435–16460. https://doi.org/10.1029/2001jb000208

Flesch, L. M., & Kreemer, C. (2010). Gravitational potential energy and regional stress and strain rate fields for continental plateaus: Examples from the central Andes and Colorado Plateau. *Tectonophysics*, *482*(1–4), 182–192. https://doi.org/10.1016/j.tecto.2009.07.014

Fletcher, H. J., & Christensen, D. H. (1996). A determination of source properties of large intraplate earthquakes in Alaska. *Pure and Applied Geophysics*, *146*(1), 21–41. https://doi.org/10.1007/bf00876668

Forsyth, D., & Uyeda, S. (1975). On the relative importance of the driving forces of plate motion. *Geophysical Journal International*, *43*(1), 163–200. https://doi.org/10.1111/j.1365-246X.1975.tb00631.x

Forte, A. M., Moucha, R., Simmons, N. A., Grand, S. P., & Mitrovica, J. X. (2010). Deep-mantle contributions to the surface dynamics of the North American continent. *Tectonophysics*, *481*(1–4), 3–15. https://doi.org/10.1016/j.tecto.2009.06.010

Fraser, K. I., Enkelmann, E., Jess, S., Gilbert, H., & Grieco, R. (2021). Resolving the Cenozoic history of rock exhumation along the Central Rocky Mountain trench using apatite low-temperature thermochronology. *Tectonics*, *40*(10), e2021TC006847. https://doi.org/10.1029/2021TC006847

Freymueller, J. T., Woodard, H., Cohen, S. C., Cross, R., Elliott, J., Larsen, C. F., et al. (2008). Active deformation processes in Alaska, based on 15 years of GPS measurements. *Active tectonics and seismic potential of Alaska*, *179*, 1–42. https://doi.org/10.1029/179gm02

Gabrielse, H., Murphy, D. C., & Mortensen, J. K. (2006). Cretaceous and Cenozoic dextral orogen-parallel displacements, magmatism, and paleogeography, north-central Canadian Cordillera. In *Paleogeography of the North American cordillera: Evidence for and against large-scale displacements* (Vol. 46, pp. 255–276). Geological Survey of Canada.

Gephart, J. W., & Forsyth, D. W. (1984). An improved method for determining the regional stress tensor using earthquake focal mechanism data: Application to the San Fernando earthquake sequence. *Journal of Geophysical Research*, *89*(B11), 9305–9320. https://doi.org/10.1029/JB089IB11P09305

Gough, D. I., & Bell, J. S. (1981). Stress orientations from oil-well fractures in Alberta and Texas. *Canadian Journal of Earth Sciences*, *18*(3), 638–645. https://doi.org/10.1139/e81-056

Gough, D. I. (1984). Mantle upflow under North America and plate dynamics. *Nature*, *311*(5985), 428–433. https://doi.org/10.1038/311428a0

Gough, D. I., Fordjor, C. K., & Bell, J. S. (1983). A stress province boundary and tractions on the North American plate. *Nature*, *305*(5935), 619–621. https://doi.org/10.1038/305619a0

Gripp, A. E., & Gordon, R. G. (2002). Young tracks of hotspots and current plate velocities. *Geophysical Journal International*, *150*(2), 321–361. https://doi.org/10.1046/j.1365-246X.2002.01627.x

Guy, M., Patton, J., Fee, J. M., Hearne, M., Martinez, E. M., Ketchum, D., et al. (2016). *National Earthquake Information Center systems overview and integration: U.S. Geological Survey Open-File Report* (techreport). U.S. Geological Survey.

Haeussler, P. J. (2008). An overview of the neotectonics of interior Alaska: Far-field deformation from the Yakutat Microplate collision. *Geophysical Monograph Series*, *179*, 83–108. https://doi.org/10.1029/179gm05

Hardebeck, J. L., & Okada, T. (2018). Temporal stress changes caused by earthquakes: A review. *Journal of Geophysical Research: Solid Earth*, *123*(2), 1350–1365. https://doi.org/10.1002/2017jb014617

Heidbach, O., Rajabi, M., Di Giacomo, D., Harris, J., Lammers, S., Morawietz, S., et al. (2025). World stress map database release 2025 [Dataset]. *GFZ Data Services*. https://doi.org/10.5880/WSM.2025.001

Heidbach, O., Reinecker, J., Tingay, M., Müller, B., Sperner, B., Fuchs, K., & Wenzel, F. (2007). Plate boundary forces are not enough: Second- and third-order stress patterns highlighted in the World Stress Map database. *Tectonics*, *26*(6). https://doi.org/10.1029/2007TC002133

Hirschberg, H. P., Lamb, S., & Savage, M. K. (2019). Strength of an obliquely convergent plate boundary: Lithospheric stress magnitudes and viscosity in New Zealand. *Geophysical Journal International*, *216*(2), 1005–1024. https://doi.org/10.1093/gji/ggy477

Humphreys, E., & Hemphill-Haley, M. A. (1996). Causes and characteristics of Western US deformation. In *Geological Society of America Abstracts* (Vol. 28).

Hyndman, R. D. (2015). Tectonics and structure of the Queen Charlotte fault zone, Haida Gwaii, and large thrust earthquakes. *Bulletin of the Seismological Society of America*, *105*(2B), 1058–1075. https://doi.org/10.1785/0120140181

Hyndman, R. D., & Currie, C. A. (2011). Why is the North America Cordillera high? Hot backarcs, thermal isostasy, and mountain belts. *Geology*, *39*(8), 783–786. https://doi.org/10.1130/G31998.1

Kreemer, C., Blewitt, G., & Klein, E. C. (2014). A geodetic plate motion and Global Strain Rate Model [Dataset]. *Geochemistry, Geophysics, Geosystems*, *15*(10), 3849–3889. https://doi.org/10.1002/2014GC005407

Laske, G., Masters, G., Ma, Z., & Pasyanos, M. E. (2012). CRUST1.0: An updated global model of Earth's crust [Dataset]. In *Geophysical research abstracts* (Vol. 14). EGU2012-3743-1. https://igppweb.ucsd.edu/~gabi/crust1.html

Lee Armstrong, R., & Ward, P. (1991). Evolving geographic patterns of Cenozoic magmatism in the North American Cordillera: The temporal and spatial association of magmatism and metamorphic core complexes. *Journal of Geophysical Research*, *96*(B8), 13201–13224. https://doi.org/10.1029/91jb00412

Leonard, L. J., Hyndman, R. D., Mazzotti, S., Nykolaishen, L., Schmidt, M., & Hippchen, S. (2007). Current deformation in the northern Canadian Cordillera inferred from GPS measurements. *Journal of Geophysical Research*, *112*(B11), 1–15. https://doi.org/10.1029/2007JB005061

Levandowski, W., Herrmann, R. B., Briggs, R., Boyd, O., & Gold, R. (2018). An updated stress map of the continental United States reveals heterogeneous intraplate stress. *Nature Geoscience*, *11*(6), 433–437. https://doi.org/10.1038/s41561-018-0120-x

Lewis, J. C., Unruh, J. R., & Twiss, R. J. (2003). Seismogenic strain and motion of the Oregon coast block. *Geology*, *31*(2), 183–186. https://doi.org/10.1130/0091-7613(2003)031⟨0183:SSAMOT⟩2.0.CO;2

Lund Snee, J. E., & Zoback, M. D. (2020). Multiscale variations of the crustal stress field throughout North America. *Nature Communications*, *11*, 1–9. https://doi.org/10.1038/s41467-020-15841-5

Luyendyk, B. P., Kamerling, M. J., & Terres, R. (1980). Geometric model for Neogene crustal rotations in southern California. *Geological Society of America Bulletin*, *91*(4 pt 1), 211–217. https://doi.org/10.1130/0016-7606(1980)91⟨211:GMFNCR⟩2.0.CO;2

Mardia, K. V., & Jupp, P. E. (2000). In K. V. Mardia & P. E. Jupp (Eds.), *Directional statistics*. John Wiley & Sons, Inc. Hoboken, NJ, USA. https://doi.org/10.1002/9780470316979

Mazzotti, S., & Hyndman, R. D. (2002). Yakutat collision and strain transfer across the northern Canadian Cordillera. *Geology*, *30*(6), 495–498. https://doi.org/10.1130/0091-7613(2002)030<0495:ycasta>2.0.co;2

McCaffrey, R. (1992). Oblique plate convergence, slip vectors, and forearc deformation. *Journal of Geophysical Research*, *97*(B6), 8905–8915. https://doi.org/10.1029/92JB00483

McCaffrey, R. (1996). Slip partitioning at convergent plate boundaries of SE Asia. *Geological Society, London, Special Publications*, *106*(1), 3–18. https://doi.org/10.1144/GSL.SP.1996.106.01.02

McCaffrey, R., King, R. W., Payne, S. J., & Lancaster, M. (2013). Active tectonics of northwestern U.S. inferred from GPS-derived surface velocities. *Journal of Geophysical Research: Solid Earth*, *118*(2), 709–723. https://doi.org/10.1029/2012JB009473

McCaffrey, R., Long, M. D., Goldfinger, C., Zwick, P. C., Nabelek, J. L., Johnson, C. K., & Smith, C. (2000). Rotation and plate locking at the southern Cascadia subduction zone. *Geophysical Research Letters*, *27*(19), 3117–3120. https://doi.org/10.1029/2000gl011768

McCaffrey, R., Qamar, A. I., King, R. W., Wells, R., Khazaradze, G., Williams, C. A., et al. (2007). Fault locking, block rotation and crustal deformation in the Pacific Northwest. *Geophysical Journal International*, *169*(3), 1315–1340. https://doi.org/10.1111/j.1365-246X.2007.03371.x

McConeghy, J., Flesch, L., & Elliott, J. (2022). Investigating the effect of mantle flow and viscosity structure on surface velocities in Alaska using 3-D geodynamic models. *Journal of Geophysical Research: Solid Earth*, *127*(10), 1–24. https://doi.org/10.1029/2022JB024704

McKay, R., Enkelmann, E., Hadlari, T., Matthews, W., & Mouthereau, F. (2021). Cenozoic exhumation history of the Eastern Margin of the Northern Canadian Cordillera. *Tectonics*, *40*(4), e2020TC006582. https://doi.org/10.1029/2020TC006582

Molnar, P., Houseman, G. A., & Conrad, C. P. (1998). Rayleigh-Taylor instability and convective thinning of mechanically thickened lithosphere: Effects of non-linear viscosity decreasing exponentially with depth and of horizontal shortening of the layer. *Geophysical Journal International*, *133*(3), 568–584. https://doi.org/10.1046/j.1365-246X.1998.00510.x

Molnar, P., & Lyon-Caen, H. (1988). Some simple physical aspects of the support, structure, and evolution of mountain belts. *Special Papers - Geological Society of America*, *218*, 179–207. https://doi.org/10.1130/SPE218-P179

Monger, J. W. H., & Gibson, H. D. (2019). Mesozoic-Cenozoic deformation in the Canadian Cordillera: The record of a "Continental Bulldozer". *Tectonophysics*, *757*, 153–169. https://doi.org/10.1016/j.tecto.2018.12.023

NOAA National Geophysical Data Center. (2009). ETOPO1 1 arc-minute global relief model [Dataset]. https://doi.org/10.7289/V5C8276M

Padgett, J., Enkelmann, E., Kellett, D. A., Moynihan, D. P., & Stephan, T. (2025). Cenozoic faulting in the Upper Hyland River Valley, Southeastern Yukon: A thermochronological perspective. *Canadian Journal of Earth Sciences*, *62*(5), 1002–1022. https://doi.org/10.1139/cjes-2024-0147

Page, R. A., Plafker, G., & Pulpan, H. (1995). Block rotation in east-central Alaska: A framework for evaluating earthquake potential? *Geology*, *23*(7), 629. https://doi.org/10.1130/0091-7613(1995)023⟨0629:BRIECA⟩2.3.CO;2

Pana, D. I., & van der Pluijm, B. A. (2015). Orogenic pulses in the Alberta Rocky Mountains: Radiometric dating of major faults and comparison with the regional tectono-stratigraphic record. *Geological Society of America Bulletin*, *127*(3–4), 480–502. https://doi.org/10.1130/B31069.1

Parsons, T., Thompson, G. A., & Smith, R. P. (1998). More than one way to stretch a tectonic model for extension along the plume track of the Yellowstone hotspot and adjacent Basin and Range Province. *Tectonics*, *17*(2), 221–234. https://doi.org/10.1029/98tc00463

Plafker, G., & Thatcher, W. (2013). Geological and geophysical evaluation of the mechanisms of the great 1899 Yakutat Bay earthquakes. In J. T. Freymueller, P. J. Haeussler, R. L. Wesson, & G. Ekström (Eds.), *Active tectonics and seismic potential of Alaska* (pp. 215–236). American Geophysical Union. https://doi.org/10.1029/179gm12

Platt, J. P., & Becker, T. W. (2013). Kinematics of rotating panels of E–W faults in the San Andreas system: What can we tell from geodesy? *Geophysical Journal International*, *194*(3), 1295–1301. https://doi.org/10.1093/gji/ggt189

Price, R. A., & Carmichael, D. M. (1986). Geometric test for Late Cretaceous- Paleogene intracontinental transform faulting in the Canadian Cordillera. *Geology*, *14*, 468–471. https://doi.org/10.1130/0091-7613(1986)14⟨468:GTFLCI⟩2.0.CO;2

Puskas, C. M., & Smith, R. B. (2009). Intraplate deformation and microplate tectonics of the Yellowstone hot spot and surrounding western U.S. interior. *Journal of Geophysical Research*, *114*(B4). https://doi.org/10.1029/2008jb005940

Ratanaruamkarn, S., Niewiadomska-Bugaj, M., & Wang, J.-C. (2009). A new estimator of a circular median. *Communications in Statistics - Simulation and Computation*, *38*(6), 1269–1291. https://doi.org/10.1080/03610910902899950

Reiter, K., Heidbach, O., Schmitt, D., Haug, K., Ziegler, M., & Moeck, I. (2014). A revised crustal stress orientation database for Canada. *Tectonophysics*, *636*, 111–124. https://doi.org/10.1016/j.tecto.2014.08.006

Richardson, R. M., & Reding, L. M. (1991). North American plate dynamics. *Journal of Geophysical Research*, *96*(B7), 12201–12223. https://doi.org/10.1029/91JB00958

Ristau, J., Rogers, G. C., & Cassidy, J. F. (2007). Stress in western Canada from regional moment tensor analysis. *Canadian Journal of Earth Sciences*, *44*(2), 127–148. https://doi.org/10.1139/E06-057

Rosenau, M., Melnick, D., & Echtler, H. (2006). Kinematic constraints on intra-arc shear and strain partitioning in the southern Andes between 38°S and 42°S latitude. *Tectonics*, *25*(4). https://doi.org/10.1029/2005TC001943

Ruppert, N. A. (2008). Stress map for Alaska from earthquake focal mechanisms. In *Active tectonics and seismic potential of Alaska* (pp. 351–367). https://doi.org/10.1029/179GM20

Savage, M. K., Aoki, Y., Unglert, K., Ohkura, T., Umakoshi, K., Shimizu, H., et al. (2016). Stress, strain rate and anisotropy in Kyushu, Japan. *Earth and Planetary Science Letters*, *439*, 129–142. https://doi.org/10.1016/j.epsl.2016.01.005

Schaeben, H., Kroner, U., & Stephan, T. (2021). Euler Poles of tectonic plates. In B. S. D. Sagar, Q. Cheng, J. McKinley, & F. Agterberg (Eds.), *Springer Nature Switzerland AG 2021* (pp. 1–7). https://doi.org/10.1007/978-3-030-26050-7_435-1

Schaeben, H., Kroner, U., & Stephan, T. (2024). Mathematical fundamentals of spherical kinematics of plate tectonics in terms of quaternions. *Mathematical Methods in the Applied Sciences*, *47*(6), 4469–4496. https://doi.org/10.1002/mma.9823

Schutt, D. L., Porritt, R. W., Estève, C., Audet, P., Gosselin, J. M., Schaeffer, A. J., et al. (2023). Lithospheric S wave velocity variations beneath the Mackenzie Mountains and Northern Canadian Cordillera. *Journal of Geophysical Research: Solid Earth*, *128*(1), 1–13. https://doi.org/10.1029/2022JB025517

Schütt, J. M., & Whipp, D. M. (2020). Controls on Continental strain partitioning above an oblique subduction Zone, Northern Andes. *Tectonics*, *39*(4), e2019TC005886. https://doi.org/10.1029/2019TC005886

Stauder, W. (1960). The Alaska earthquake of July 10, 1958: Seismic studies. *Bulletin of the Seismological Society of America*, *50*(2), 293–322. https://doi.org/10.1785/bssa0500020293

Stephan, T. (2024). Tectonicr: Analyzing the Orientation of Maximum Horizontal Stress (Version 0.4.6) [Software]. *The Comprehensive R Archive Network*. https://doi.org/10.32614/CRAN.package.tectonicr

Stephan, T., Enkelmann, E., & Kroner, U. (2023). Analyzing the horizontal orientation of the crustal stress adjacent to plate boundaries. *Scientific Reports*, *13*(1), 15590. https://doi.org/10.1038/s41598-023-42433-2

Tikoff, B., & Teyssier, C. (1994). Strain modeling of displacement-field partitioning in transpressional orogens. *Journal of Structural Geology*, *16*(11), 1575–1588. https://doi.org/10.1016/0191-8141(94)90034-5

Townend, J., Sherburn, S., Arnold, R., Boese, C., & Woods, L. (2012). Three-dimensional variations in present-day tectonic stress along the Australia–Pacific plate boundary in New Zealand. *Earth and Planetary Science Letters*, *353–354*, 47–59. https://doi.org/10.1016/j.epsl.2012.08.003

Unruh, J., & Humphrey, J. (2017). Seismogenic deformation between the Sierran microplate and Oregon Coast block, California, USA. *Geology*, *45*(5), 415–418. https://doi.org/10.1130/G38696.1

van der Pluijm, B. A., Vrolijk, P. J., Pevear, D. R., Hall, C. M., & Solum, J. (2006). Fault dating in the Canadian Rocky Mountains: Evidence for late Cretaceous and early Eocene orogenic pulses. *Geology*, *34*(10), 837–840. (Ar/Ar paper wo die verschiedenen Thrust faults datiert wurden). https://doi.org/10.1130/G22610.1

Waite, G. P., & Smith, R. B. (2004). Seismotectonics and stress field of the Yellowstone volcanic plateau from earthquake first-motions and other indicators. *Journal of Geophysical Research*, *109*(B2). https://doi.org/10.1029/2003jb002675

Wang, K. (2000). Stress–strain "paradox", plate coupling, and forearc seismicity at the Cascadia and Nankai subduction zones. *Tectonophysics*, *319*(4), 321–338. https://doi.org/10.1016/S0040-1951(99)00301-7

Wdowinski, S. (1998). A theory of intraplate tectonics. *Journal of Geophysical Research*, *103*(3), 5037–5059. https://doi.org/10.1029/97JB03390

Wells, R. E., Blakely, R. J., & Bemis, S. (2020). Northward migration of the Oregon forearc on the Gales Creek fault. *Geosphere*, *16*(2), 660–684. https://doi.org/10.1130/ges02177.1

Wells, R. E., Weaver, C. S., & Blakely, R. J. (1998). Fore-arc migration in Cascadia and its neotectonic significance. *Geology*, *26*(8), 759. https://doi.org/10.1130/0091-7613(1998)026⟨0759:FAMICA⟩2.3.CO;2

Wüstefeld, A., Bokelmann, G., Barruol, G., & Montagner, J.-P. (2009). Identifying global seismic anisotropy patterns by correlating shear-wave splitting and surface-wave data [Dataset]. *Physics of the Earth and Planetary Interiors*, *176*(3–4), 198–212. https://doi.org/10.1016/j.pepi.2009.05.006

Zoback, M. L. (1992a). First- and second-order patterns of stress in the lithosphere: The World Stress Map Project. *Journal of Geophysical Research*, *97*(B8), 11703–11728. https://doi.org/10.1029/92JB00132

Zoback, M. L. (1992b). Stress field constraints on intraplate seismicity in eastern North America. *Journal of Geophysical Research*, *97*(B8), 11761–11782. https://doi.org/10.1029/92jb00221

Zoback, M. L., & Mooney, W. D. (2003). Lithospheric buoyancy and continental intraplate stresses. *International Geology Review*, *45*(2), 95–118. https://doi.org/10.2747/0020-6814.45.2.95

Zoback, M. L., Zoback, M. D., Adams, J., Assumpção, M., Bell, S., Bergman, E. A., et al. (1989). Global patterns of tectonic stress. *Nature*, *341*(6240), 291–298. https://doi.org/10.1038/341291a0

References From the Supporting Information

Becker, T. W., Kellogg, J. B., Ekström, G., & O'Connell, R. J. (2003). Comparison of azimuthal seismic anisotropy from surface waves and finite strain from global mantle-circulation models. *Geophysical Journal International*, *155*(2), 696–714. https://doi.org/10.1046/j.1365-246x.2003.02085.x

Blackman, D. K., Wenk, H.-R., & Kendall, J. M. (2002). Seismic anisotropy of the upper mantle 1. Factors that affect mineral texture and effective elastic properties. *Geochemistry, Geophysics, Geosystems*, *3*(9), 1–24. https://doi.org/10.1029/2001gc000248

Courtier, A. M., Gaherty, J. B., Revenaugh, J., Bostock, M. G., & Garnero, E. J. (2010). Seismic anisotropy associated with continental lithosphere accretion beneath the CANOE array. *Northwestern Canada. Geology*, *38*(10), 887–890. https://doi.org/10.1130/G31120.1

Durand, D., & Greenwood, J. A. (1957). Random unit vectors II: Usefulness of Gram-Charlier and related series in approximating distributions. *The Annals of Mathematical Statistics*, *28*(4), 978–986. https://doi.org/10.1214/aoms/1177706798

Estève, C., Audet, P., Schaeffer, A. J., Schutt, D., Aster, R. C., & Cubley, J. (2020). The upper mantle structure of Northwestern Canada from teleseismic body wave tomography. *Journal of Geophysical Research: Solid Earth*, *125*(2), e2019JB018837. https://doi.org/10.1029/2019JB018837

Fisher, N. I. (1993). *Statistical analysis of circular data*. Cambridge University Press.

Global Volcanism Program. (2024). Volcanoes of the World (Version 5.2.1) [Dataset] (Database). https://doi.org/10.5479/si.GVP.VOTW5-2024.5.2

Holtzman, B. K., & Kendall, J. (2010). Organized melt, seismic anisotropy, and plate boundary lubrication. *Geochemistry, Geophysics, Geosystems*, *11*(12). https://doi.org/10.1029/2010gc003296

Jung, H., & Karato, S.-I. (2001). Water-Induced fabric transitions in olivine. *Science*, *293*(5534), 1460–1463. https://doi.org/10.1126/science.1062235

Kaminski, E., & Ribe, N. M. (2002). Timescales for the evolution of seismic anisotropy in mantle flow. *Geochemistry, Geophysics, Geosystems*, *3*(8), 1–17. https://doi.org/10.1029/2001gc000222

Lewis, T. J., Hyndman, R. D., & Flück, P. (2003). Heat flow, heat generation, and crustal temperatures in the northern Canadian Cordillera: Thermal control of tectonics. *Journal of Geophysical Research*, *108*(B6). https://doi.org/10.1029/2002jb002090

Mainprice, D., Barruol, G., & Ismaïl, W. B. (2000). The Seismic anisotropy of the Earth's mantle: From single crystal to polycrystal. In *Earth's deep interior: Mineral physics and tomography from the atomic to the global Scale* (pp. 237–264). American Geophysical Union. https://doi.org/10.1029/gm117p0237

Nicolas, A., & Christensen, N. I. (1987). Formation of anisotropy in upper mantle peridotites: A review. In *Composition, structure and dynamics of the lithosphere-asthenosphere System* (pp. 111–123). American Geophysical Union. https://doi.org/10.1029/gd016p0111

Polet, J., & Kanamori, H. (2002). Anisotropy beneath California: Shear wave splitting measurements using a dense broadband array. *Geophysical Journal International*, *149*(2), 313–327. https://doi.org/10.1046/j.1365-246X.2002.01630.x

Silver, P. G. (1996). Seismic anisotropy beneath the continents: Probing the depths of geology. *Annual Review of Earth and Planetary Sciences*, *24*(24), 385–432. https://doi.org/10.1146/annurev.earth.24.1.385

Silver, P. G., & Chan, W. W. (1988). Implications for continental structure and evolution from seismic anisotropy. *Nature*, *335*(6185), 34–39. https://doi.org/10.1038/335034a0

Tarayoun, A., Audet, P., Mazzotti, S., & Ashoori, A. (2017). Architecture of the crust and uppermost mantle in the northern Canadian Cordillera from receiver functions. *Journal of Geophysical Research: Solid Earth*, *122*(7), 5268–5287. https://doi.org/10.1002/2017jb014284

Tommasi, A., Mainprice, D., Canova, G., & Chastel, Y. (2000). Viscoplastic self-consistent and equilibrium-based modeling of olivine lattice preferred orientations: Implications for the upper mantle seismic anisotropy. *Journal of Geophysical Research*, *105*(B4), 7893–7908. https://doi.org/10.1029/1999jb900411

Venereau, C. M. A., Martin-Short, R., Bastow, I. D., Allen, R. M., & Kounoudis, R. (2019). The role of variable slab dip in driving mantle flow at the Eastern edge of the Alaskan subduction margin: Insights from shear-wave splitting. *Geochemistry, Geophysics, Geosystems*, *20*(5), 2433–2448. https://doi.org/10.1029/2018GC008170

Yang, W., & Hauksson, E. (2013). The tectonic crustal stress field and style of faulting along the Pacific North America Plate boundary in Southern California. *Geophysical Journal International*, *194*(1), 100–117. https://doi.org/10.1093/gji/ggt113

Ziegler, M. O., & Heidbach, O. (2017). Matlab script Stress2Grid v1.1 [Software] (techreport). *GFZ German Research Centre for Geosciences*. https://doi.org/10.5880/wsm.2017.002